



Zircon U–Pb dating and *in-situ* Hf isotopic analysis of Permian peraluminous granite in the Lhasa terrane, southern Tibet: Implications for Permian collisional orogeny and paleogeography

Di-Cheng Zhu^{a,*}, Xuan-Xue Mo^a, Yaoling Niu^b, Zhi-Dan Zhao^a, Li-Quan Wang^c, Gui-Tang Pan^c, Fu-Yuan Wu^d

^a State Key Laboratory of Geological Processes and Mineral Resources, China University of Geosciences, 29# Xue-Yuan Road, Haidian District, Beijing 100083, PR China

^b Department of Earth Sciences, Durham University, Durham DH1 3LE, UK

^c Chengdu Institute of Geology and Mineral Resources, Chengdu 610082, PR China

^d Institute of Geology and Geophysics, Chinese Academy of Sciences, Beijing 100029, PR China

ARTICLE INFO

Article history:

Received 28 August 2008

Received in revised form 12 January 2009

Accepted 18 January 2009

Available online 27 January 2009

Keywords:

Strongly peraluminous granite
Permian syncollisional orogeny
Gondwana reconstruction
Lhasa terrane
Southern Tibet

ABSTRACT

The Lhasa terrane has long been interpreted as a simple tectonic block rifted from Gondwana during the late Paleozoic and then drifted northward before finally amalgamating with the Qiangtang terrane during the Early Cretaceous. In this paper we document Permian peraluminous granites near Pikang in the southern margin of the central Lhasa terrane, close to the recently documented Songdo eclogite of Permian age. Zircon SHRIMP and LA-ICPMS U–Pb dating for a Pikang granite sample gives an identical crystallization age of about 263 Ma and a wide age range of inherited zircons (283–2141 Ma). *In situ* Hf isotopic analyses for 20 zircons of 263 Ma yielded $\varepsilon_{\text{Hf}(t)}$ values of -4.5 to $+1.9$. The Pikang granites have high A/CNK values (≥ 1.08) and high normative corundum (1.3–2.0%), indicative of peraluminous S-type granite. They are characterized by moderately negative Eu anomalies ($\text{Eu}/\text{Eu}^* = 0.48\text{--}0.61$), and strongly negative Ba, Nb, Sr, P and Ti anomalies. The granites have high $\varepsilon_{\text{Nd}(t)}$ values (-6.4 to -6.0) and low initial $^{87}\text{Sr}/^{86}\text{Sr}$ ratios (0.7082–0.7096) relative to melts derived from mature continental crust. These rocks are interpreted to have been generated by mixing between mantle melts and their induced melting of mature crustal materials. We interpret the Pikang peraluminous granite magmatism, the regional angular unconformity between the Middle and the Upper Permian and the eclogite of the same metamorphic age (~ 262 Ma) from the same geotectonic location to represent different products of a common event in time and space. We tentatively term this common event as syncollisional orogeny, i.e., “the Permian Gangdese Orogeny”. We further hypothesize that the orogeny may be genetically associated with the collision between the Lhasa terrane and the northern margin of Australia, following the closure of the Paleo-Tethyan Ocean south of the Lhasa terrane.

© 2009 Elsevier B.V. All rights reserved.

1. Introduction

The Lhasa terrane located on the southern Tibetan Plateau (Fig. 1a) is widely considered not only as an archetype of a Cenozoic orogen as a result of India–Asia continental collision, but also as an Andean-type active continental margin that developed during the northward subduction of the Neo-Tethyan ocean lithosphere along the Indus–Yarlung Zangbo suture zone (IYZSZ) before the onset of India–Asia collision (Maluski et al., 1982; Xu et al., 1985; Coulon et al., 1986; XBGMR, 1991; Copeland et al., 1995; Yin and Harrison, 2000; Chung et al., 2005; Chu et al., 2006; Wen et al., 2008a; Zhu et al., 2008a,b, 2009). Numerous studies over the past decades on the Cenozoic geology have led to our current understanding of the India–Asia collision-related tectonic processes and the formation of the Hima-

ayas and Tibetan Plateau (e.g., England and Searle, 1986; Yin et al., 1994; Murphy et al., 1997; Kapp et al., 2005, 2007; He et al., 2007; Wang et al., 2008). Although there has been a growing attention to the pre-Cenozoic history of the Lhasa terrane that led to the recognition of Late Triassic, Early Jurassic, and Cretaceous Gangdese orogenic events (Chu et al., 2006; Guynn et al., 2006; Liu et al., 2006a; Zhang et al., 2007; Zhu et al., 2008a, 2009), our knowledge on the nature and pre-Cenozoic history of the Lhasa terrane remains rather limited. For example, the tectonic history and paleogeography of the Lhasa terrane during the Permian remain unanswered and conflicting views exist (Leier et al., 2007; Zhu et al., 2008b, submitted for publication-b). Conventionally, the Lhasa terrane has been interpreted as a single tectonic block that developed in a rifting/back-arc extensional setting related to the separation of the Qiangtang terrane from Gondwana during the late Paleozoic (Dewey et al., 1988; Pearce and Mei, 1988; Leeder et al., 1988; Yin and Harrison, 2000; Metcalfe, 2002; Booth et al., 2004; Kapp et al., 2005, 2007; Leier et al., 2007), whereas recent studies

* Corresponding author. Tel./fax: +86 10 8232 2094.
E-mail address: dchengzhu@163.com (D.-C. Zhu).

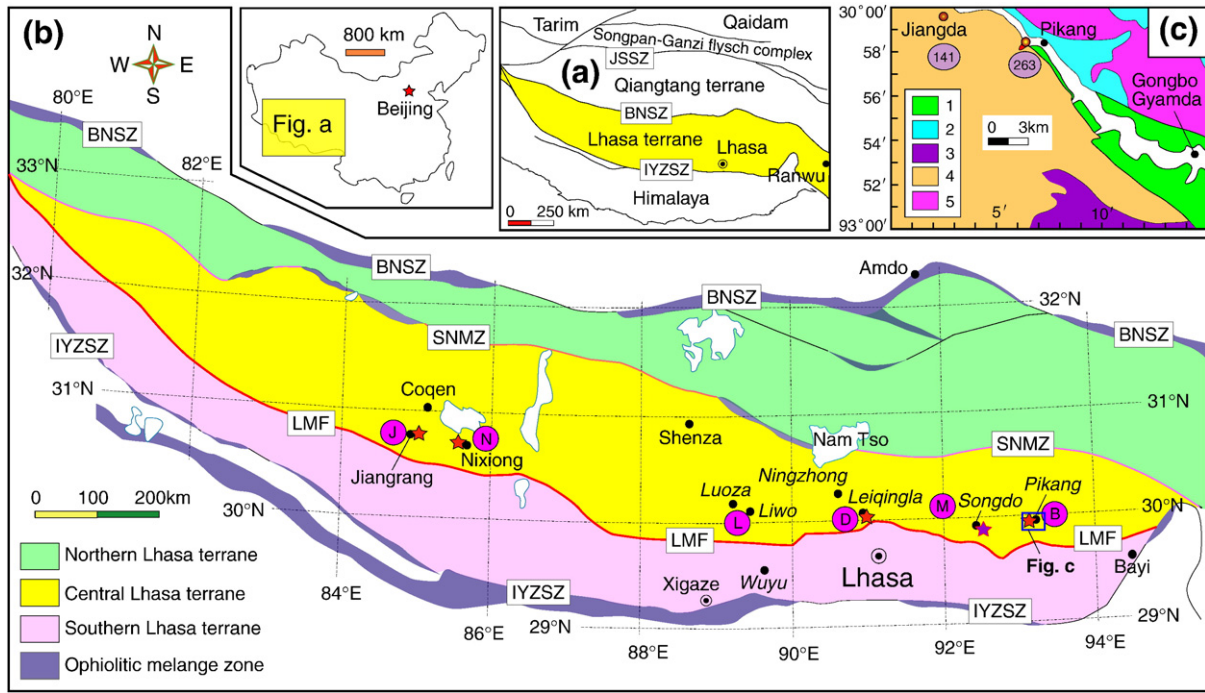


Fig. 1. (a) Tectonic outline of the Tibetan Plateau showing the study area (Zhu et al., 2008a). (b) Tectonic framework of the Lhasa terrane showing the major tectonic subdivisions (Zhu et al., submitted for publication-b), the localities of Permian igneous rocks (red stars) and angular unconformity between the Middle and the Upper Permian (pink circles with letter, also shown in Fig. 7). JSSZ = Jinsha suture zone; BNSZ = Bangong–Nujiang suture zone; SNMZ = Shiquanhe–Nam Tso Mélange Zone; LMF = Luobadui–Milashan Fault; IYZSZ = Indus–Yarlung Zangbo Suture Zone. B = Bahe; M = Menba; D = Leiqingla; L = Liwo; N = Nixiong; J = Jiangrang. (c) Simplified geological map of the NW Gongbo Gyamda County (Yin et al., 2003) showing the location of the Pikang granites investigated in this study. 1 = Pre-Ordovician metasedimentary rocks; 2 = Upper Carboniferous–Lower Permian metasedimentary rocks; 3 = Lower Jurassic Yeba Formation; 4 = Early Cretaceous granitoids; 5 = Late Cretaceous granitoids. (For interpretation of the references to color in this figure legend, the reader is referred to the web version of this article.)

argue that the Lhasa terrane represents a volcanic arc system during the Permian (Pan et al., 2006; Zhu et al., submitted for publication-b).

The above contrasting views have resulted in variable paleogeographic reconstructions of the Lhasa terrane during the late Paleozoic, including (1) the Lhasa terrane was positioned adjacent to Greater India until the Late Permian (Golonka and Ford, 2000; Metcalfe, 2002; Scotese, 2004) or even the Late Triassic (Golonka, 2007), (2) the Lhasa terrane was located within the Paleo-Tethyan Ocean during the Late Permian (Enkin et al., 1992; Ziegler et al., 1997; Scotese et al., 1999; Stampfli and Borel, 2002), and (3) the Lhasa terrane may have been a separate intra-Tethyan oceanic block during the Early to Middle Permian (Zhu et al., submitted for publication-b). The most likely reason for these contrasting views is the limited data that have been accumulated from the Lhasa terrane in different stages. For example, the first two scenarios cannot explain the presence of paleontologically age-constrained Permian arc volcanic rocks (Zhu et al., submitted for publication-b) and the Songdo eclogite (Yang et al., 2009) recently recognized in the Lhasa terrane. The third hypothesis has incorporated these new observations. However, it remains unclear how the Early to Middle Permian subduction system of the Lhasa terrane might have evolved to Late Permian and how the location of the Lhasa terrane may have changed with time.

In this paper we report U–Pb age and Hf isotope data from zircons and whole-rock major and trace element, and Sr–Nd isotope data on granitoid samples from Pikang village in northwestern Gongbo Gyamda County of the Lhasa terrane (Fig. 1b). These data reveal the presence of strongly peraluminous granitoids (i.e., molecular $Al_2O_3/(CaO + Na_2O + K_2O)$ or $A/CNK \geq 1.1$) of Permian age, which, in combination with the known arc-type volcanism, high-pressure metamorphism and other geologic observations, provide solid lines of evidence for the existence of a Permian Gangdese orogeny in the Lhasa terrane and place new constraints on the paleogeography of the Lhasa terrane throughout the Permian.

2. Geological background and samples

Geologically, the autonomous Tibet (the southern portion of the Greater Tibetan Plateau) comprises, from north to south, the following four blocks or terranes: the Songpan–Ganzi flysch complex, Qiangtang terrane, Lhasa terrane, and the Himalaya. These blocks are separated by the Jinsha (JSSZ), Bangong–Nujiang (BNSZ), and IYZSZ suture zones, representing Paleo-, Meso-, and Neo-Tethyan oceanic relicts, respectively (Fig. 1a) (Yin and Harrison, 2000).

The Lhasa terrane, which is bounded to the north by the BNSZ and to the south by the IYZSZ (Fig. 1a), can be divided into northern, central, and southern subterrane, separated by the Shiquan River–Nam Tso Mélange Zone (SNMZ) and Luobadui–Milashan Fault (LMF), respectively (Fig. 1b). The northern Lhasa terrane is inferred to be underlain by Cambrian crystalline basement, which has been reported only from the Amdo area (Amdo orthogneiss; Fig. 1b) (Xu et al., 1985; Dewey et al., 1988; Guynn et al., 2006). The main rock units exposed in this terrane are Jurassic–Cretaceous sedimentary and igneous rocks (Leeder et al., 1988; Yin et al., 1988; Pan and Ding, 2004; Zhang et al., 2004; Leier et al., 2007; Zhu et al., 2008a). The central Lhasa terrane consists predominantly of a Carboniferous–Permian metasedimentary sequence and a Late Jurassic–Early Cretaceous volcano-sedimentary sequence, with minor Ordovician, Silurian, and Triassic limestones (Leeder et al., 1988; Yin et al., 1988; Pan and Ding, 2004; Kapp et al., 2005; Ji et al., 2007; Leier et al., 2007; Zhu et al., 2008a) and rare Precambrian strata (Hu et al., 2005). The southern Lhasa terrane is dominated by the Cretaceous to early Tertiary Gangdese batholiths and Linzizong volcanic succession with minor Triassic–Cretaceous volcano-sedimentary rocks (Leeder et al., 1988; Pearce and Mei, 1988; Pan and Ding, 2004; He et al., 2007; Leier et al., 2007; Mo et al., 2007; Wen et al., 2008a; Zhu et al., 2008a). The Permian volcanic rocks are exposed discretely along the southern margin of the central Lhasa terrane from western Coqen County to central Leiqingla area (Fig. 1b) and

eastern Ranwu Town (Fig. 1a) (Zhu et al., submitted for publication-b). Mesozoic and Cenozoic igneous rocks are widespread in the Lhasa terrane. These rocks define five magmatic episodes that took place at 190–175, 120–110, 100–80, 65–45, and 25–10 Ma, with two magmatic flare-ups at ca. 110 and 50 Ma (Wen et al., 2008a; Zhu et al., 2008b).

The Lhasa terrane is traditionally thought to have rifted from Gondwana during the Late Triassic and then drifted northward before finally amalgamating with the Qiangtang terrane during the Early Cretaceous (Yin and Harrison, 2000; Metcalfe, 2002; Kapp et al., 2005; Leier et al., 2007). However, the Early to Middle Permian arc-type magmatism (Zhu et al., submitted for publication-b), and the Songdo

eclogite of Permian age (Yang et al., 2009) recently identified in the southern margin of the central Lhasa terrane (Fig. 1b), along with Permian extension-type magmatism in the Tethyan Himalaya suggest that the Lhasa terrane may have been an entirely separate intra-Tethyan oceanic block during the Early to Middle Permian (Zhu et al., submitted for publication-b).

Samples investigated in this study were collected near Pikang village, ~20 km northwest of Gongbo Gyamda County (Fig. 1b and c) in the central Lhasa terrane (N29°58.381', E93°06.447'). The Pikang granite occurs as relicts (of variable size) (Fig. 2a) or apophysis (about 80 m-wide) within the Early Cretaceous granite that intruded the pre-

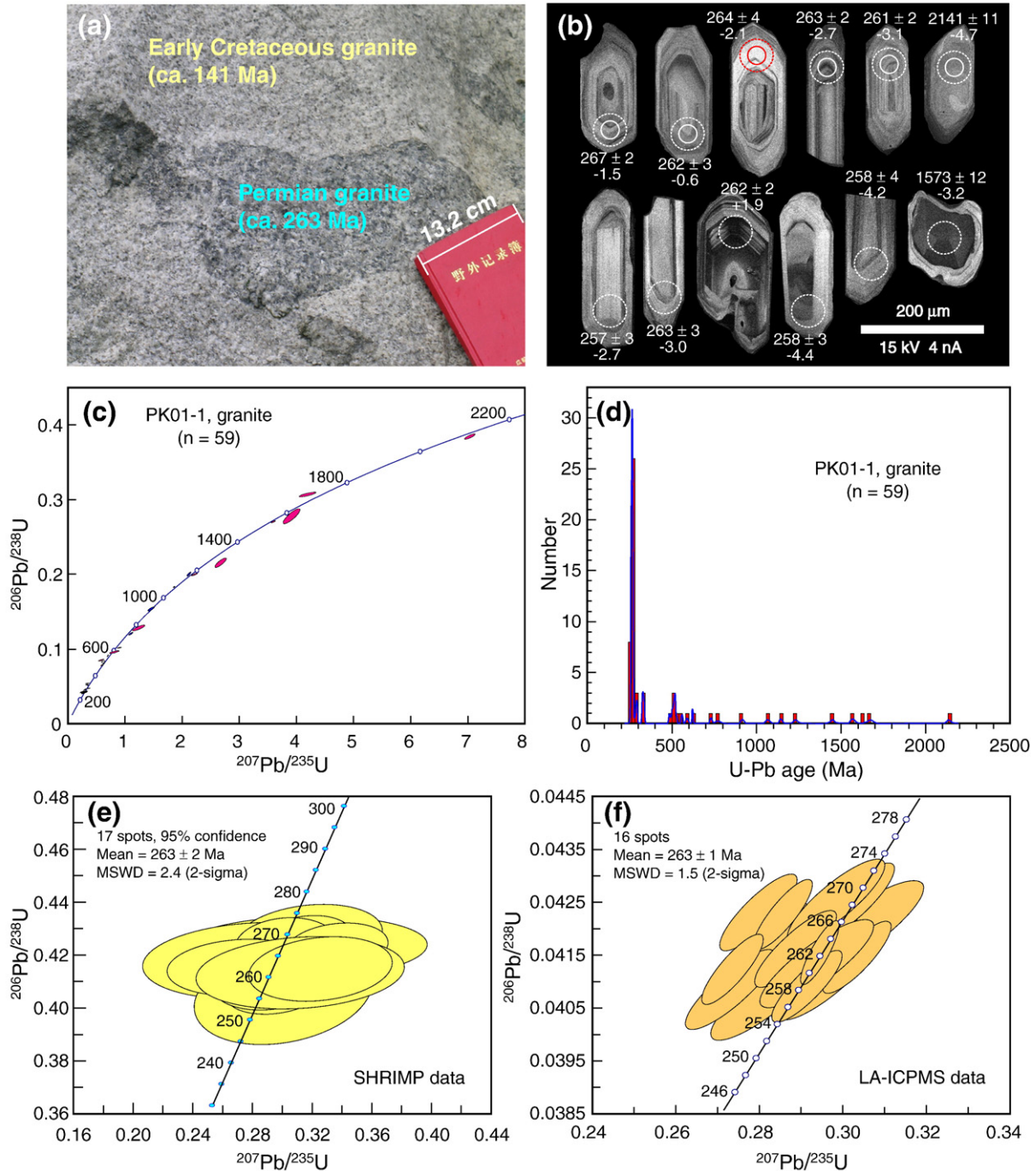


Fig. 2. (a) Field photograph showing the Permian Pikang granites occur as relicts of variable size within Early Cretaceous granitoids near Pikang village. (b) Cathodoluminescence (CL) images of representative zircon. Solid and dashed circles indicate the locations of SHRIMP U-Pb dating and LA-ICPMS U-Pb dating and Hf analyses, respectively. The U-Pb age dates and $\epsilon_{\text{Hf}(t)}$ values are given for each spot. (c) U-Pb concordia diagram of zircons from sample PK01-1. (d) Age-probability plot of zircons from sample PK01-1. (e) Concordia plot for single zircon analyzed by SHRIMP U-Pb. (f) Concordia plot for single zircon analyzed by LA-ICPMS U-Pb.

Table 1

Zircon SHRIMP U–Pb data of a Pikang granite sample (PK01-1), Lhasa terrane.

Analysis	²⁰⁶ Pb _c	Th	U	Th/U	²⁰⁶ Pb*	Isotopic ratios (±1σ)						Isotopic ages (±1σ)							
	%	ppm	ppm		ppm	²⁰⁷ Pb*/ ²⁰⁶ Pb*	²⁰⁷ Pb*/ ²³⁵ U	²⁰⁶ Pb*/ ²³⁸ U	²³⁸ U/ ²⁰⁶ Pb*	²⁰⁷ Pb/ ²⁰⁶ Pb	²⁰⁶ Pb*/ ²³⁸ U	²⁰⁸ Pb/ ²³² Th							
1.1	0.64	65	214	0.31	7.61	0.0509	0.0025	0.289	0.015	0.04117	0.00040	24.29	0.24	238	120	260	3	215	15
2.1	1.00	75	216	0.35	7.79	0.0476	0.0035	0.273	0.020	0.04154	0.00042	24.08	0.24	81	180	262	3	259	20
3.1	1.70	81	195	0.42	7.19	0.0539	0.0059	0.314	0.035	0.04225	0.00051	23.67	0.28	367	250	267	3	259	26
4.1	1.75	56	168	0.34	6.13	0.0489	0.0054	0.282	0.031	0.04178	0.00058	23.94	0.34	144	250	264	4	243	31
5.1	0.42	65	279	0.23	9.97	0.0571	0.0034	0.327	0.020	0.04148	0.00050	24.11	0.29	495	130	262	3	311	27
6.1	0.54	45	324	0.14	11.40	0.0529	0.0024	0.297	0.014	0.04067	0.00037	24.59	0.22	324	100	257	2	272	31
7.1	1.36	79	90	0.88	7.48	0.0634	0.0042	0.834	0.057	0.09540	0.00134	10.48	0.15	721	140	588	8	640	29
8.1	0.63	40	408	0.10	14.40	0.0543	0.0023	0.306	0.013	0.04083	0.00034	24.49	0.21	385	95	258	2	293	40
9.1	1.55	99	160	0.62	5.77	0.0550	0.0050	0.313	0.029	0.04130	0.00054	24.21	0.31	413	200	261	3	241	17
10.1	1.15	71	165	0.43	6.11	0.0543	0.0034	0.319	0.020	0.04267	0.00051	23.44	0.28	383	140	269	3	272	16
11.1	0.17	272	403	0.68	28.00	0.0584	0.0010	0.650	0.012	0.08065	0.00050	12.40	0.08	546	37	500	3	533	7
12.1	0.07	152	284	0.54	93.50	0.1332	0.0008	7.045	0.061	0.38350	0.00238	2.61	0.02	2141	11	2093	11	2126	22
13.1	0.72	93	200	0.47	7.34	0.0540	0.0024	0.316	0.014	0.04240	0.00042	23.59	0.24	371	98	268	3	268	10
14.1	0.73	81	285	0.28	10.20	0.0541	0.0026	0.308	0.015	0.04125	0.00037	24.24	0.22	375	110	261	2	256	16
15.1	1.08	53	149	0.36	5.23	0.0541	0.0043	0.302	0.025	0.04050	0.00077	24.69	0.47	376	180	256	5	275	23
16.1	0.67	55	626	0.09	22.60	0.0526	0.0022	0.302	0.013	0.04169	0.00028	23.99	0.16	312	93	263	2	241	46
17.1	0.94	46	327	0.14	11.80	0.0542	0.0025	0.310	0.015	0.04154	0.00037	24.07	0.21	379	100	262	2	276	27
18.1	0.48	53	335	0.16	12.20	0.0580	0.0024	0.338	0.014	0.04226	0.00038	23.67	0.21	529	91	267	2	306	28
19.1	1.14	346	172	2.01	12.60	0.0521	0.0026	0.607	0.030	0.08450	0.00093	11.83	0.13	291	110	523	5	498	9
20.1	0.48	60	93	0.64	10.30	0.0715	0.0037	1.258	0.072	0.12760	0.00268	7.84	0.16	972	110	774	16	732	38
21.1	0.30	122	572	0.21	49.80	0.0663	0.0018	0.923	0.026	0.10096	0.00046	9.91	0.05	815	57	620	3	661	42
22.1	0.21	106	389	0.27	26.10	0.0576	0.0014	0.620	0.016	0.07804	0.00062	12.81	0.10	515	54	484	4	470	19
23.1	0.18	107	185	0.58	48.80	0.0998	0.0022	4.210	0.097	0.30600	0.00211	3.27	0.02	1620	41	1721	10	1632	140
24.1	0.20	738	898	0.82	208	0.0973	0.0006	3.613	0.025	0.26936	0.00084	3.71	0.01	1573	12	1538	4	1480	13
25.1	0.10	105	296	0.36	70.40	0.1029	0.0008	3.931	0.098	0.27700	0.00665	3.61	0.09	1678	14	1576	33	1546	45
26.1	0.06	850	951	0.89	149	0.0749	0.0004	1.878	0.013	0.18179	0.00056	5.50	0.02	1067	12	1077	3	1048	6
27.1	1.08	88	308	0.29	11.30	0.0504	0.0041	0.294	0.024	0.04238	0.00030	23.60	0.17	212	190	268	2	231	25
28.1	0.13	552	956	0.58	68.40	0.0569	0.0009	0.653	0.010	0.08322	0.00027	12.02	0.04	487	33	515	2	502	5
29.1	0.80	96	416	0.23	18.70	0.0504	0.0024	0.360	0.017	0.05189	0.00032	19.27	0.12	211	110	326	2	310	27
30.1	1.18	106	243	0.44	11.30	0.0504	0.0029	0.372	0.022	0.05352	0.00037	18.68	0.13	211	130	336	2	306	17
31.1	0.19	159	229	0.69	39.20	0.0815	0.0011	2.234	0.034	0.19880	0.00111	5.03	0.03	1234	27	1169	6	1157	16
32.1	0.15	59	122	0.48	22.50	0.0911	0.0013	2.694	0.065	0.21450	0.00408	4.66	0.09	1449	27	1253	22	1633	40
33.1	0.99	57	346	0.16	14.00	0.0596	0.0034	0.384	0.022	0.04669	0.00031	21.42	0.14	590	120	294	2	308	49
34.1	0.58	123	239	0.51	8.50	0.0515	0.0038	0.292	0.022	0.04114	0.00030	24.31	0.18	262	170	260	2	262	13

²⁰⁶Pb_c denotes the proportion of common ²⁰⁶Pb in total measured ²⁰⁶Pb. *Denotes radiogenic lead.

Ordovician, Upper Carboniferous to Lower Permian, and Lower Jurassic metasedimentary successions as batholiths (Fig. 1c). The Pikang granites are coarse- to medium-grained, undeformed and

typically contain alkali-feldspar (30–40%), quartz (30–45%), plagioclase (5–15%), biotite (5–10%) and accessory minerals (<1%) including zircon and Fe–Ti oxides. Alkali-feldspar shows distinct K- and Na-

Table 2

Zircon LA-ICPMS U–Pb data of a Pikang granite sample (PK01-1), Lhasa terrane.

Analysis	U	Th	Pb*	Th/U	Common-Pb corrected isotopic ratios (±1σ)						Common-Pb corrected isotopic ages (±1σ)					
	(ppm)	(ppm)	(ppm)		²⁰⁷ Pb*/ ²⁰⁶ Pb*	²⁰⁷ Pb*/ ²³⁵ U	²⁰⁶ Pb*/ ²³⁸ U	²³⁸ U/ ²⁰⁶ Pb	²⁰⁷ Pb/ ²⁰⁶ Pb	²⁰⁶ Pb*/ ²³⁸ U	²⁰⁸ Pb/ ²³² Th					
-01	188	81	9	0.43	0.05164	0.00113	0.303	0.006	0.04251	0.00048	270	28	268	3	268	5
-02	283	47	12	0.16	0.04906	0.00128	0.282	0.007	0.04169	0.00051	151	35	263	3	252	6
-03	204	164	52	0.80	0.07802	0.00090	2.143	0.023	0.19933	0.00202	1147	10	1172	11	1163	8
-04	303	129	14	0.43	0.05171	0.00103	0.291	0.006	0.04090	0.00045	273	24	258	3	260	4
-05	191	50	9	0.26	0.05180	0.00124	0.324	0.007	0.04544	0.00054	277	31	286	3	285	6
-06	591	255	31	0.43	0.05144	0.00056	0.294	0.003	0.04154	0.00040	261	10	262	2	262	2
-07	223	58	10	0.26	0.05092	0.00136	0.298	0.008	0.04252	0.00052	237	36	268	3	265	6
-08	185	132	9	0.71	0.05234	0.00139	0.296	0.007	0.04102	0.00050	300	35	259	3	263	6
-09	394	64	17	0.16	0.04802	0.00108	0.280	0.006	0.04230	0.00048	100	30	267	3	251	5
-10	208	64	10	0.31	0.05521	0.00238	0.311	0.013	0.04088	0.00069	421	61	258	4	275	10
-11	262	122	26	0.47	0.05784	0.00084	0.722	0.010	0.09055	0.00093	524	14	559	5	552	6
-12	232	54	10	0.23	0.04856	0.00130	0.273	0.007	0.04084	0.00050	127	37	258	3	245	6
-13	298	56	13	0.19	0.05036	0.00116	0.289	0.006	0.04161	0.00048	212	30	263	3	258	5
-14	687	55	59	0.08	0.05481	0.00057	0.622	0.006	0.08234	0.00079	404	10	510	5	491	4
-15	298	72	13	0.24	0.05110	0.00127	0.293	0.007	0.04162	0.00050	245	33	263	3	261	5
-16	232	43	38	0.19	0.05293	0.00077	0.374	0.005	0.05132	0.00052	326	15	323	3	323	4
-17	191	63	10	0.33	0.05195	0.00187	0.322	0.011	0.04493	0.00066	283	52	283	4	283	8
-18	146	83	27	0.57	0.07002	0.00199	1.478	0.038	0.15309	0.00174	929	60	918	10	921	16
-19	183	70	25	0.39	0.06786	0.00155	1.124	0.023	0.12013	0.00127	864	49	731	7	765	11
-20	428	58	19	0.14	0.04907	0.00083	0.286	0.005	0.04226	0.00044	151	19	267	3	255	4
-21	388	407	21	1.05	0.04821	0.00089	0.274	0.005	0.04122	0.00044	110	22	260	3	246	4
-22	178	72	9	0.40	0.05282	0.00164	0.306	0.009	0.04210	0.00056	321	43	266	3	271	7
-23	313	142	16	0.45	0.05309	0.00098	0.303	0.005	0.04145	0.00045	333	21	262	3	269	4
-24	379	176	17	0.46	0.05020	0.00159	0.282	0.008	0.04071	0.00055	204	45	257	3	252	7
-25	192	110	9	0.57	0.05159	0.00163	0.294	0.009	0.04133	0.00055	267	45	261	3	262	7

*Radiogenic lead. Isotopic ratios and ages were corrected by common lead, following the methods reported by Andersen (2002).

feldspar perthitic texture and microcline twinning. Some alkali-feldspar occurs as megacrysts. Quartz occurs as interstitial grains and quartz-feldspar intergrowths are common. Plagioclase occurs as euhedral laths and biotite as independent grains with rare muscovite.

3. Analytical methods

Zircons were separated from the Pikang granite (sample PK01-1) by heavy-liquid and magnetic methods in the Laboratory of the Geological Team of Hebei Province, China. Cathodoluminescence images were used to check the internal structures of individual zircon grains and to select positions for analyses. *In situ* zircon U–Pb dating was performed using the sensitive high-resolution ion microprobe (SHRIMP) at the Beijing SHRIMP Center following the procedure by Liu et al. (2006b) and laser ablation inductively coupled plasma mass spectrometry (LA-ICPMS) at the Institute of Geology and Geophysics, Chinese Academy of Sciences in Beijing following the procedure by Xie et al. (2008). $^{206}\text{Pb}/^{238}\text{U}$ ages were used for <1000 Ma, and $^{207}\text{Pb}/^{206}\text{Pb}$ ages were used for >1000 Ma. The zircon U–Pb dating results are presented in Tables 1 and 2.

In situ Hf isotope analysis was done on zircon grains using LA-ICPMS with a beam size of 60 μm and laser pulse frequency of 8 Hz.

Details of instrumental conditions and data acquisition were given in Wu et al. (2006) and Xie et al. (2008). During the analysis, $^{176}\text{Hf}/^{177}\text{Hf}$ ratios of the zircon standard (91500) were 0.282286 ± 12 ($2\sigma_n$, $n=21$). The zircon Hf isotope data are given in Table 3. The $\varepsilon_{\text{Hf}(t)}$ values (parts in 10^4 deviation of initial Hf isotope ratios between the zircon sample and the chondritic reservoir) and $T_{\text{DM}}^{\text{zircon}}$ (zircon Hf isotope crustal model ages based on a depleted-mantle source and an assumption that the protolith of the zircon's host magma has the average continental crustal $^{176}\text{Lu}/^{177}\text{Hf}$ ratio of 0.015) were calculated following Griffin et al. (2002) using the ^{176}Lu decay constant given in Blichert-Toft and Albarède (1997). Our conclusions would not be affected if other decay constants were used.

Whole-rock compositions were analyzed in the State Key Laboratory of Continental Dynamics, Northwest University (Xi'an, China) by XRF for major element oxides with analytical uncertainty usually better than 5%, and by ICP-MS for trace elements with analytical uncertainty better than 5–10%. An internal standard was used to monitor mass drift during analysis (see Gao et al., 2002 for analytical details). Whole-rock Nd and Sr isotopic compositions were determined using a multicollector Finnigan MAT-261 mass spectrometer operated in static multicollector mode at the same laboratory. Sr and Nd isotopic fractionation was corrected to $^{86}\text{Sr}/^{88}\text{Sr} = 0.1194$ and

Table 3
Hf isotopic data for zircons from a Pikang granite sample (PK01-1), Lhasa terrane.

Analysis	Age	$^{176}\text{Yb}/^{177}\text{Hf}$	$\pm 2\sigma$	$^{176}\text{Lu}/^{177}\text{Hf}$	$\pm 2\sigma$	$^{176}\text{Hf}/^{177}\text{Hf}$	$\pm 2\sigma$	$^{176}\text{Hf}/^{177}\text{Hf}_t$	$\varepsilon_{\text{Hf}(0)}$	$\varepsilon_{\text{Hf}(t)}$	T_{DM} (Ma)	$T_{\text{DM}}^{\text{zircon}}$ (Ma)	$f_{\text{Lu/Hf}}$
1	263	0.031418	0.000944	0.001022	0.000031	0.282550	0.000016	0.282545	-7.8	-2.2	993	1430	-0.97
2	261	0.037953	0.001197	0.001228	0.000038	0.282606	0.000017	0.282600	-5.9	-0.4	920	1308	-0.96
3	266	0.043845	0.001003	0.001412	0.000028	0.282491	0.000016	0.282484	-9.9	-4.3	1088	1565	-0.96
4	1620	0.035238	0.000185	0.001205	0.000006	0.281917	0.000013	0.281880	-30.2	4.5	1886	2043	-0.96
5	1573	0.042363	0.000143	0.002174	0.000020	0.281757	0.000012	0.281693	-35.9	-3.2	2163	2486	-0.93
6	1678	0.029306	0.000596	0.000970	0.000016	0.281565	0.000013	0.281535	-42.7	-6.4	2358	2766	-0.97
7	263	0.024780	0.000147	0.000815	0.000004	0.282553	0.000016	0.282549	-7.7	-2.1	984	1421	-0.98
8	262	0.021013	0.000503	0.000681	0.000017	0.282595	0.000015	0.282591	-6.3	-0.6	923	1327	-0.98
9	260	0.028390	0.000323	0.000903	0.000011	0.282604	0.000014	0.282599	-6.0	-0.4	915	1311	-0.97
10	258	0.054444	0.001056	0.001754	0.000032	0.282500	0.000015	0.282492	-9.6	-4.3	1085	1533	-0.95
11	262	0.038460	0.000744	0.001243	0.000023	0.282543	0.000017	0.282537	-8.1	-2.5	1009	1448	-0.96
12	265	0.030540	0.000366	0.000983	0.000012	0.282542	0.000015	0.282537	-8.1	-2.5	1004	1446	-0.97
13	267	0.041607	0.000785	0.001424	0.000028	0.282485	0.000014	0.282478	-10.1	-4.5	1097	1578	-0.96
14	500	0.014224	0.000074	0.000456	0.000002	0.282146	0.000013	0.282142	-22.1	-11.3	1536	2180	-0.99
15	2141	0.014187	0.000130	0.000451	0.000005	0.281334	0.000014	0.281316	-50.8	-4.7	2638	2976	-0.99
16	326	0.031644	0.000432	0.000976	0.000013	0.282540	0.000014	0.282534	-8.2	-1.2	1006	1414	-0.97
17	268	0.035368	0.000109	0.001117	0.000002	0.282555	0.000015	0.282549	-7.7	-2.0	990	1418	-0.97
18	261	0.045068	0.000196	0.001409	0.000006	0.282529	0.000014	0.282522	-8.6	-3.1	1034	1483	-0.96
19	515	0.044539	0.000962	0.001378	0.000030	0.282012	0.000013	0.281999	-26.9	-16.0	1762	2488	-0.96
20	336	0.034163	0.001396	0.001167	0.000044	0.282703	0.000018	0.282696	-2.4	4.7	781	1044	-0.96
21	1234	0.016695	0.000155	0.000542	0.000005	0.281646	0.000015	0.281633	-39.8	-12.9	2223	2834	-0.98
22	1449	0.028337	0.000344	0.000906	0.000013	0.282271	0.000019	0.282246	-17.7	13.6	1381	1339	-0.97
23	257	0.026568	0.000362	0.000863	0.000011	0.282539	0.000014	0.282535	-8.2	-2.7	1005	1457	-0.97
24	263	0.039741	0.000911	0.001265	0.000029	0.282540	0.000015	0.282533	-8.2	-2.7	1015	1456	-0.96
25	263	0.031025	0.000541	0.000997	0.000018	0.282530	0.000014	0.282525	-8.6	-3.0	1021	1476	-0.97
26	267	0.023229	0.000129	0.000764	0.000005	0.282567	0.000015	0.282563	-7.3	-1.5	964	1388	-0.98
27	264	0.033369	0.000969	0.001108	0.000032	0.282539	0.000014	0.282534	-8.2	-2.6	1011	1455	-0.97
28	294	0.022072	0.000333	0.000761	0.000011	0.282140	0.000014	0.282136	-22.3	-16.0	1556	2324	-0.98
29	542	0.024023	0.000131	0.000759	0.000004	0.282391	0.000013	0.282384	-13.5	-1.8	1208	1613	-0.98
30	258	0.043476	0.000477	0.001413	0.000013	0.282499	0.000016	0.282492	-9.7	-4.2	1077	1552	-0.96
31	774	0.038139	0.000592	0.001292	0.000019	0.282138	0.000018	0.282120	-22.4	-6.0	1581	2054	-0.96
32	620	0.019993	0.000393	0.000697	0.000014	0.282078	0.000016	0.282069	-24.6	-11.2	1640	2264	-0.98
33	484	0.019776	0.000075	0.000715	0.000003	0.282227	0.000016	0.282221	-19.3	-8.9	1435	2015	-0.98
34	1147	0.026752	0.000566	0.001008	0.000021	0.282110	0.000015	0.282088	-23.4	1.2	1609	1885	-0.97
35	258	0.039209	0.001611	0.001311	0.000052	0.282494	0.000014	0.282488	-9.8	-4.4	1081	1562	-0.96
36	262	0.046157	0.001036	0.001491	0.000030	0.282671	0.000014	0.282664	-3.6	1.9	833	1163	-0.96
37	510	0.017952	0.000266	0.000682	0.000011	0.282077	0.000014	0.282070	-24.6	-13.6	1641	2333	-0.98
38	323	0.022538	0.000972	0.000927	0.000035	0.282299	0.000015	0.282294	-16.7	-9.8	1342	1955	-0.97
39	918	0.032593	0.000504	0.001159	0.000017	0.282173	0.000015	0.282153	-21.2	-1.6	1528	1888	-0.97
40	731	0.021582	0.000061	0.000771	0.000002	0.282256	0.000016	0.282245	-18.3	-2.5	1397	1802	-0.98

*: $\varepsilon_{\text{Hf}(t)} = 10,000 \times \{[(^{176}\text{Hf}/^{177}\text{Hf})_s - (^{176}\text{Lu}/^{177}\text{Hf})_s \times (e^{\lambda t} - 1)] / [(^{176}\text{Hf}/^{177}\text{Hf})_{\text{CHUR},0} - (^{176}\text{Lu}/^{177}\text{Hf})_{\text{CHUR}} \times (e^{\lambda t} - 1)] - 1\}$.

$T_{\text{DM}} = 1/\lambda \times \ln\{1 + [(^{176}\text{Hf}/^{177}\text{Hf})_s - (^{176}\text{Hf}/^{177}\text{Hf})_{\text{DM}}] / [(^{176}\text{Lu}/^{177}\text{Hf})_s - (^{176}\text{Lu}/^{177}\text{Hf})_{\text{DM}}]\}$.

$T_{\text{DM}}^{\text{zircon}} = T_{\text{DM}} - (T_{\text{DM}} - t) \times \{f_{\text{cc}} - f_s\} / (f_{\text{cc}} - f_{\text{DM}})$.

$f_{\text{Lu/Hf}} = (^{176}\text{Lu}/^{177}\text{Hf})_s / (^{176}\text{Lu}/^{177}\text{Hf})_{\text{CHUR}} - 1$.

where, $\lambda = 1.867 \times 10^{-11} \text{ year}^{-1}$ (Soderlund et al., 2004); $(^{176}\text{Lu}/^{177}\text{Hf})_s$ and $(^{176}\text{Hf}/^{177}\text{Hf})_s$ are the measured values of the samples; $(^{176}\text{Lu}/^{177}\text{Hf})_{\text{CHUR},0} = 0.0332$ and $(^{176}\text{Hf}/^{177}\text{Hf})_{\text{CHUR},0} = 0.282772$ (Blichert-Toft and Albarède, 1997); $(^{176}\text{Lu}/^{177}\text{Hf})_{\text{DM}} = 0.0384$ and $(^{176}\text{Hf}/^{177}\text{Hf})_{\text{DM}} = 0.28325$ (Griffin et al., 2000); $(^{176}\text{Lu}/^{177}\text{Hf})_{\text{mean crust}} = 0.015$; $f_{\text{cc}} = [(^{176}\text{Lu}/^{177}\text{Hf})_{\text{mean crust}} / (^{176}\text{Lu}/^{177}\text{Hf})_{\text{CHUR}}] - 1$; $f_s = f_{\text{Lu/Hf}}$; $f_{\text{DM}} = [(^{176}\text{Lu}/^{177}\text{Hf})_{\text{DM}} / (^{176}\text{Lu}/^{177}\text{Hf})_{\text{CHUR}}] - 1$; t = crystallization time of zircon.

Table 4

Whole-rock major, trace element and Sr–Nd isotopic data of the Pikang granites, Lhasa terrane.

Sample	PK01-1	PK01-2	PK01-3	PK01-4	PK01-5	PK01-6	GBJD-1*	GBJD-2*	GBJD-3*
<i>XRF – major element (wt.%)</i>									
SiO ₂	73.37	72.84	73.02	71.61	73.00	73.64	70.47	72.47	71.80
TiO ₂	0.31	0.33	0.33	0.31	0.29	0.29	0.34	0.35	0.35
Al ₂ O ₃	13.67	13.56	13.63	14.31	13.78	13.39	14.76	13.73	14.03
TFe ₂ O ₃	2.55	2.60	2.58	2.58	2.35	2.34	2.46	2.72	2.70
MnO	0.04	0.04	0.04	0.04	0.04	0.04	0.04	0.05	0.05
MgO	0.66	0.69	0.67	0.68	0.56	0.61	0.59	0.64	0.62
CaO	1.33	1.29	1.27	1.30	1.40	1.20	1.34	1.36	1.35
Na ₂ O	2.74	2.73	2.71	2.83	2.91	2.57	3.30	2.91	2.98
K ₂ O	5.10	5.25	5.25	5.51	4.69	5.24	4.99	4.48	4.82
P ₂ O ₅	0.15	0.13	0.13	0.14	0.12	0.13	0.16	0.15	0.16
LOI	0.41	0.50	0.50	0.33	0.42	0.50	0.75	0.67	0.67
Total	100.33	99.96	100.13	99.64	99.56	99.95	99.19	99.52	99.52
A/CNK	1.10	1.08	1.10	1.10	1.11	1.11	1.11	1.14	1.12
<i>Normative CIPW (%)</i>									
Quartz	34.0	33.1	33.4	30.3	34.4	35.2	28.2	34.3	31.9
Anorthite	5.77	5.72	5.61	5.75	6.33	5.29	5.79	5.91	5.82
Albite	23.2	23.3	23.1	24.1	24.9	21.9	28.4	25.0	25.6
Orthoclase	30.2	31.2	31.2	32.8	28.0	31.2	30.0	26.8	28.9
Corundum	1.54	1.31	1.45	1.61	1.64	1.57	1.88	1.99	1.83
Hypersthene	2.75	2.82	2.75	2.77	2.47	2.55	3.92	3.86	4.09
Ilmenite	0.59	0.63	0.63	0.59	0.56	0.55	0.66	0.67	0.67
Magnetite	1.57	1.62	1.60	1.64	1.43	1.44	0.72	1.07	0.90
Apatite	0.35	0.30	0.30	0.33	0.28	0.30	0.39	0.36	0.38
Zircon	0.04	0.04	0.04	0.04	0.04	0.03	0.04	0.04	0.05
Total	100.0	100.0	100.0	100.0	100.0	100.0	100.0	100.0	100.0
<i>ICP-MS – trace element (ppm)</i>									
Sc	3.95	4.19	4.24	4.29	3.96	3.82	4.01	4.12	4.15
V	22.9	23.4	23.5	23.5	20.2	21.6	25.3	25.4	24.9
Cr	15.0	13.8	16.6	15.7	13.2	12.3	11.4	12.9	13.3
Co	3.31	4.36	4.89	3.93	3.44	3.59			
Ni	7.32	7.49	8.51	7.37	6.26	6.85			
Ga	19.1	19.5	19.8	20.5	19.7	18.6			
Ge	1.51	1.58	1.54	1.59	1.62	1.48			
Rb	143	197	197	227	207	209	195	200	204
Sr	168	173	171	186	155	174	170	157	172
Y	30.2	27.6	27.5	26.7	31.5	26.4	26.3	28.3	27.6
Zr	178	192	185	184	177	150	188	209	224
Nb	29.3	29.5	30.4	30.2	26.4	27.1	27.2	29.6	28.8
Cs	4.28	8.81	8.71	11.6	10.8	9.45	11.9	12.2	11.8
Ba	408	403	395	540	266	491	302	340	352
La	45.8	44.0	44.2	46.5	43.8	42.1	49.5	50.9	51.7
Ce	87.4	84.2	83.8	87.6	84.7	78.6	92.1	95.1	96.2
Pr	9.28	8.91	8.77	9.19	8.87	8.34	10.1	10.6	10.5
Nd	33.8	32.2	31.6	32.7	31.3	29.5	35.2	36.4	36.9
Sm	6.36	5.99	5.97	6.11	5.91	5.54	6.08	6.51	6.32
Eu	0.95	1.00	1.00	1.11	0.88	1.03	1.15	1.00	1.10
Gd	5.53	5.27	5.17	5.28	5.24	4.83	5.84	6.10	6.05
Tb	0.90	0.85	0.84	0.83	0.88	0.79	0.88	0.91	0.89
Dy	5.29	4.96	4.94	4.91	5.33	4.65	4.86	5.03	4.98
Ho	1.08	0.99	0.99	0.98	1.11	0.95	0.91	0.99	0.98
Er	2.83	2.63	2.60	2.55	3.04	2.51	2.60	2.80	2.74
Tm	0.41	0.38	0.38	0.37	0.46	0.37	0.36	0.39	0.38
Yb	2.60	2.47	2.47	2.40	2.98	2.36	2.28	2.48	2.44
Lu	0.37	0.35	0.35	0.33	0.42	0.33	0.33	0.35	0.35
Hf	4.75	5.11	5.02	5.03	5.02	4.07	4.59	5.21	5.53
Ta	2.36	2.76	2.83	3.27	2.65	2.40	2.83	2.91	2.71
Pb	22.5	27.3	27.4	29.8	31.5	28.2	22.0	27.0	24.5
Th	20.3	22.2	22.7	22.5	25.5	20.2	17.7	19.7	20.4
U	3.39	2.26	2.32	2.80	3.03	2.14	1.67	1.94	1.99
(La/Yb) _N	12.7	12.8	12.8	13.9	10.5	12.8	15.6	14.7	15.2
Eu/Eu*	0.49	0.54	0.55	0.60	0.48	0.61	0.59	0.49	0.54
<i>Sr–Nd isotope compositions</i>									
⁸⁷ Rb/ ⁸⁶ Sr	2.46	3.30	3.33	3.53	3.86	3.47			
⁸⁷ Sr/ ⁸⁶ Sr	0.71875	0.72142	0.72177	0.72193	0.72266	0.72175			
±2σ	0.000003	0.000003	0.000003	0.000004	0.000004	0.000004			
¹⁴⁷ Sm/ ¹⁴⁴ Nd	0.1137	0.1124	0.1141	0.1129	0.1141	0.1138			
¹⁴³ Nd/ ¹⁴⁴ Nd	0.512187	0.512176	0.512182	0.512182	0.512186	0.512169			
±2σ	0.000008	0.000008	0.000010	0.000008	0.000006	0.000010			
(⁸⁷ Sr/ ⁸⁶ Sr) _t	0.7096	0.7091	0.7093	0.7088	0.7082	0.7088			
ε _{Nd(t)}	−6.0	−6.2	−6.1	−6.1	−6.1	−6.4			
T _{DM}	1469	1465	1482	1463	1476	1496			

(continued on next page)

Table 4 (continued)

Sr–Nd isotope compositions						
$T_{DM}^{206Pb/238U}$	1523	1536	1532	1527	1525	1551
$(^{143}Nd/^{144}Nd)_t$	0.51199	0.51198	0.51199	0.51199	0.51199	0.51197

LOI = loss on ignition. A/CNK = molecular $Al_2O_3/(CaO + Na_2O + K_2O)$. $Eu/Eu^* = Eu_N/(Sm_N \times Gd_N)^{1/2}$, the subscript N denotes chondrite-normalized (Sun and McDonough, 1989) values. Corrected formula as follows: $(^{87}Sr/^{86}Sr)_t = (^{87}Sr/^{86}Sr)_{sample} + ^8Rb/^{86}Sr(e^{\lambda t} - 1)$, $\lambda = 1.42 \times 10^{-11} a^{-1}$; $(^{143}Nd/^{144}Nd)_t = (^{143}Nd/^{144}Nd)_{sample} + (^{147}Sm/^{144}Nd)_m \times (e^{\lambda t} - 1)$, $\epsilon_{Nd(t)} = [(^{143}Nd/^{144}Nd)_{sample} / (^{143}Nd/^{144}Nd)_{CHUR(t)} - 1] \times 10^4$, $(^{143}Nd/^{144}Nd)_{CHUR(t)} = 0.512638 - 0.1967 \times (e^{\lambda t} - 1)$. $T_{DM} = 1/\lambda \times \ln \{1 + [(^{143}Nd/^{144}Nd)_{sample} - 0.51315] / [(^{147}Sm/^{144}Nd)_{sample} - 0.21317]\}$, $\lambda_{Sm-Nd} = 6.54 \times 10^{-12} a^{-1}$; T_{DM} is calculated using the same assumption formulation as Keto and Jacobsen (1987). Data marked by * are from Liao et al. (to be submitted).

$^{146}Nd/^{144}Nd = 0.7219$, respectively. The average $^{143}Nd/^{144}Nd$ ratio of the La Jolla standard measured during the sample runs is 0.511862 ± 5 (2-sigma), and the average $^{87}Sr/^{86}Sr$ ratio of the NBS987 standard is 0.710236 ± 16 (2-sigma). Total procedural Sr and Nd blanks are < 1 ng and < 50 pg, respectively. Analytical details were given in Zhang et al. (2002). Table 4 gives the analytical data.

4. Results

4.1. Zircon U–Pb age

Zircons from sample PK01-1 are light pink or colorless and prismatic (~100–300 μm long), and show clear oscillatory zoning and inherited cores (Fig. 2b). Of the 34 zircon grains dated by SHRIMP system in this sample, 17 grains with clear oscillatory zoning have Th/U ratios varying from 0.1 to 0.6 and yield concordant $^{206}Pb/^{238}U$ ages of 256 to 269 Ma (Table 1; Fig. 2c and d) with a mean of 263 ± 2 Ma (MSWD = 2.4) (Fig. 2e). Twenty-five zircon grains from this same sample were analyzed using LA-ICPMS (Table 2). These latter analyses yield Th/U ratios of 0.1–1.0 and concordant or slightly discordant ages. The 16 analyses on zircon grains with magmatic oscillatory zoning yield concordant or near-concordant $^{206}Pb/^{238}U$ ages between 257 and 268 Ma (Table 2; Fig. 2c and d) with a mean of 263 ± 1 Ma (MSWD = 1.5) (Fig. 2f), which is identical to the SHRIMP result within error. Both the SHRIMP and LA-ICPMS results are consistent with the magmatic crystallization age of the Pikang granite being about 263 Ma, slightly postdating the paleontologically age-constrained Middle Permian Leiqingla high-alumina basalts in the same belt (Fig. 1b; Zhu et al., submitted for publication-b). The remaining 20 analyses on inherited cores plot along or close to the concordia line (Fig. 2c) and yield a large age range from 283 to 2141 Ma (Fig. 2d). These inherited zircon cores are interpreted as reflecting the tectonomagmatic history of the terrane.

4.2. Zircon Hf isotope

Of the 59 dated zircon grains from sample PK01-1, 40 were analyzed for Hf isotope ratios (Table 3). The youngest cluster with $^{206}Pb/^{238}U$ age of ~263 Ma (20 analyses) yielded $\epsilon_{Hf(t)}$ values from -4.5 to $+1.9$ (average = -2.4 ; Fig. 3a), and a narrow range of Hf isotope crustal model ages (T_{DM}^C) from 1.2 to 1.6 Ga (Fig. 3b). This differs from the crustal type Hf isotope composition (-16.8 to -3.3 ; Zhu et al., submitted for publication-a) (Fig. 3a) of zircons from the Late Triassic peraluminous granites in Luoza area of the central Lhasa terrane (Fig. 1b). Of the remaining inherited zircons (i.e., those with U–Pb ages between ca. 283 and 2141 Ma), 19 show varying $\epsilon_{Hf(t)}$ values from -16.0 to $+4.6$ (Fig. 3a), yielding dispersed T_{DM}^C model ages from 1.0 to 3.0 Ga (Table 3; Fig. 3b). The inherited zircon grain of 1449 Ma in this sample has $\epsilon_{Hf(t)}$ value of $+13.6$ that is close to the mean value of the depleted mantle at that time (Fig. 3b), suggesting an origin from a mantle-derived magma.

4.3. Whole-rock major and trace element data

The Pikang granite samples show uniform major element compositions, with $SiO_2 = 70.5$ – 73.6 wt.%, $CaO = 1.2$ – 1.4 % and $CaO/Na_2O = 0.41$ – 0.49 (Table 4). In comparison with the Miocene peraluminous

granites in North Himalaya ($K_2O/Na_2O = 0.9$ – 1.4 ; Zhang et al., 2004), they are more enriched in K_2O ($K_2O/Na_2O = 1.51$ – 2.03). The high A/CNK values (1.08–1.14), presence of normative corundum (1.3–2.0%) and absence of normative diopside of these rocks are consistent with them being strongly peraluminous S-type granites with mature crustal protoliths.

The Pikang granite samples display moderately negative Eu anomalies ($Eu/Eu^* = 0.48$ – 0.61) and fractionated REE patterns characterized by $(La/Yb)_N$ ratios of 10.5–15.6 (Table 4) that differ distinctly from the Late Triassic peraluminous granites in Luoza area of the central Lhasa terrane (Fig. 4a; Zhang et al., 2007) and the Miocene peraluminous granites in the North Himalaya (Fig. 4a; Zhang et al., 2004). In primitive mantle-normalized spidergram (Fig. 4b), the Pikang granite samples show weak but significant negative Ba, Nb, Sr,

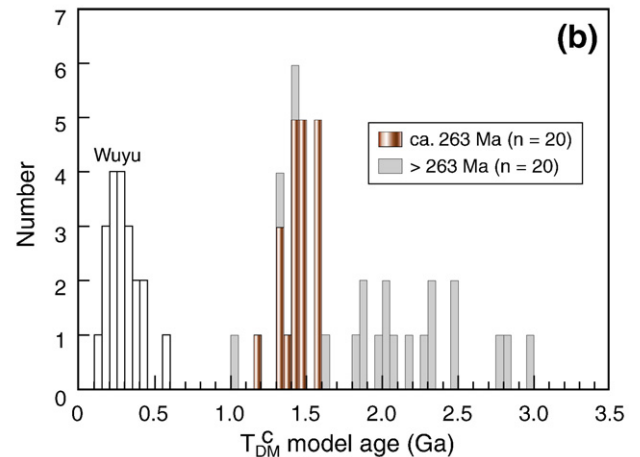
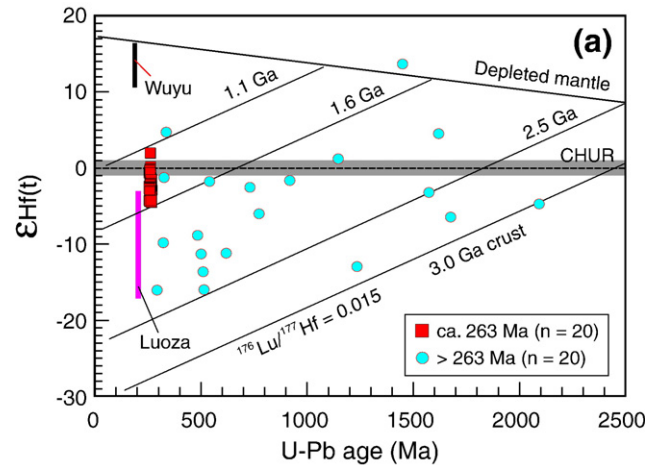


Fig. 3. (a) Plots of $\epsilon_{Hf(t)}$ (the parts in 10^4 deviation of initial Hf isotope ratios between the zircon sample and the chondritic reservoir) vs. U–Pb ages. (b) Histogram of T_{DM}^C (zircon Hf isotope crustal model age) for zircons from sample PK01-1. For comparison, also plotted are Early Jurassic granitoid from Wuyu basin (Chu et al., 2006) and Late Triassic Luoza strongly peraluminous granite from the central Lhasa terrane (Zhu et al., submitted for publication-a).

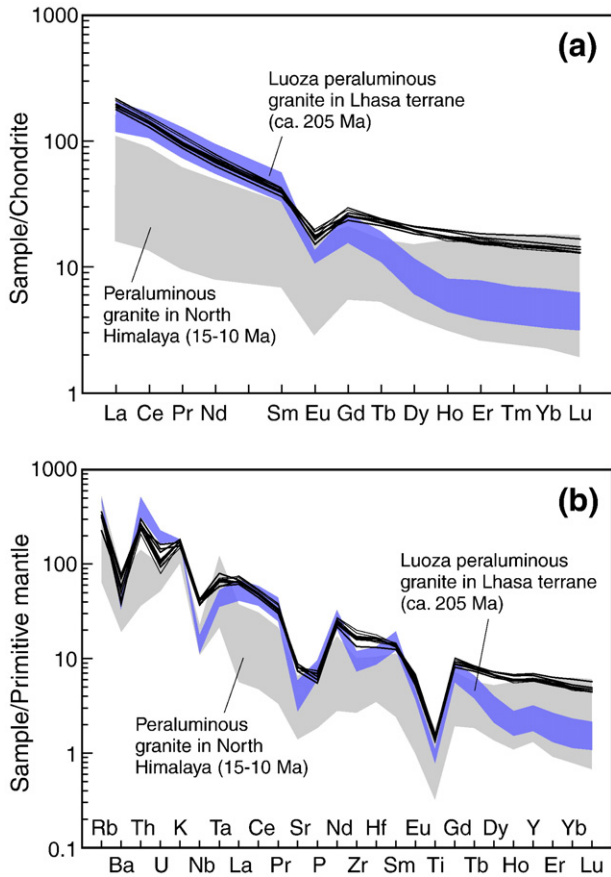


Fig. 4. Chondrite-normalized REE and primitive-mantle-normalized trace element patterns for the Pikang granites, Luoza strongly peraluminous granite in Lhasa terrane (205 Ma; Zhang et al., 2007), and North Himalayan strongly peraluminous granite (15–10 Ma; Zhang et al., 2004). Data for normalization and plotting are from Sun and McDonough (1989). Note that the Pikang granites show distinct patterns from other rock suites.

P and Ti anomalies relative to the Luoza strongly peraluminous granites in the Lhasa terrane and the Miocene peraluminous granites in the North Himalaya.

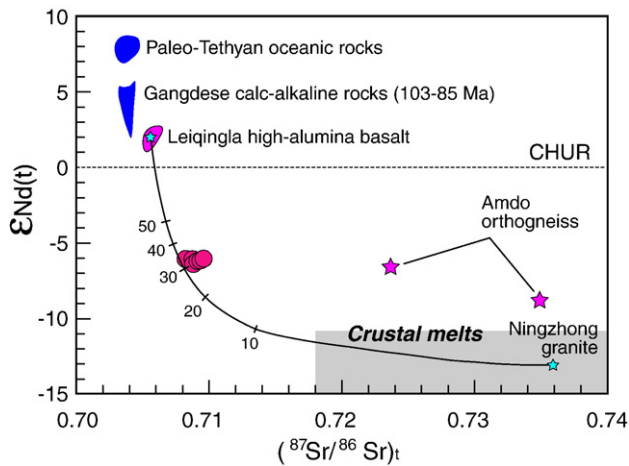


Fig. 5. $\epsilon_{Nd(t)}$ vs. $(^{87}Sr/^{86}Sr)_t$ diagram comparing the Pikang granites and other rock suites from the Lhasa terrane. Data sources are Paleo-Tethyan oceanic rocks (Li et al., 2008), Gangdese calc-alkaline rocks (103–85 Ma) (Wen et al., 2008b), Leiqingla high-alumina basalt (average values for modeling: Nd = 20 ppm, $\epsilon_{Nd(t)} = 2.0$, Sr = 6872 ppm, $(^{87}Sr/^{86}Sr)_t = 0.7056$; Zhu et al., submitted for publication-b), Ningzhong strongly peraluminous granites (gray field) as a proxy for crustal melt (average values for modeling: Nd = 11.8 ppm, $\epsilon_{Nd(t)} = -13.1$, Sr = 26.7 ppm, $(^{87}Sr/^{86}Sr)_t = 0.73586$; Liu et al., 2006a), and Amdo orthogneiss (Xu et al., 1985). Note that the Sr and Nd isotopic compositions of the Pikang granites can be explained by crustal melts mixed with ~30% Leiqingla high-alumina basaltic melts.

4.4. Whole-rock Sr and Nd isotopic data

As a whole, the Pikang granite samples have significantly higher $\epsilon_{Nd(t)}$ values (–6.4 to –6.0) and lower initial $^{87}Sr/^{86}Sr$ ratios (0.7082–0.7096) than the Early Jurassic strongly peraluminous granites in Ningzhong area of the central Lhasa terrane (Fig. 5; Liu et al., 2006a) and the Miocene strongly peraluminous granites in the North Himalaya (not shown in Fig. 5) (Zhang et al., 2004), where the rocks have ancient crustal isotopic signatures. This implies some significant mantle contributions towards the Pikang granite petrogenesis (see below). The Pikang granite samples have a narrow two-stage Nd model age of 1523 to 1551 Ma, similar to the T_{DM} model ages of ~263 Ma zircons (see Fig. 3 and discussion above).

5. Discussion

5.1. Origin of the Pikang granite

As presented above, the Pikang granites are geochemically distinct from the Late Triassic peraluminous granites in Luoza area of the central Lhasa terrane and the Miocene peraluminous granites in the North Himalaya in having higher HREE abundances, moderately fractionated REE patterns (Fig. 4), and lower initial $^{87}Sr/^{86}Sr$ ratios and higher $\epsilon_{Nd(t)}$ values (Fig. 5; Zhang et al., 2004). These geochemical differences suggest that the origin of the Pikang granites differs from that of the Late Triassic Luoza peraluminous granites in the central Lhasa terrane and the Miocene peraluminous granites in the North Himalaya, which have been attributed to mica dehydration melting of argillaceous source rocks in the crust (Zhang et al., 2004, 2007).

All the analyzed Pikang granite samples are peraluminous, placing a first-order constraint that their sources most likely include melts of supracrustal rocks. Previous studies suggest that peraluminous rocks could be produced by (i) melting of metapelite and metagreywacke, including cases of basalt magma admixture (White and Chappell, 1988; Patino Douce, 1995; Sylvester, 1998; Eyal et al., 2004); (ii) partial melting of tonalite and granodiorite at pressures ≥ 8 kbar with clinopyroxene in restite (Patino Douce, 1997, 1999); and (iii) amphibole fractionation from relatively primitive low-Ca metaluminous granitic melts (Bonin, 1998). While these processes are all possible for the Pikang granite petrogenesis, several lines of evidence suggest that melts parental to the Pikang granites are best explained by mixing between melts derived from Al_2O_3 -rich rocks (e.g., metapelite, including terrigenous sediments or upper crustal materials) and minor basalt-derived melts.

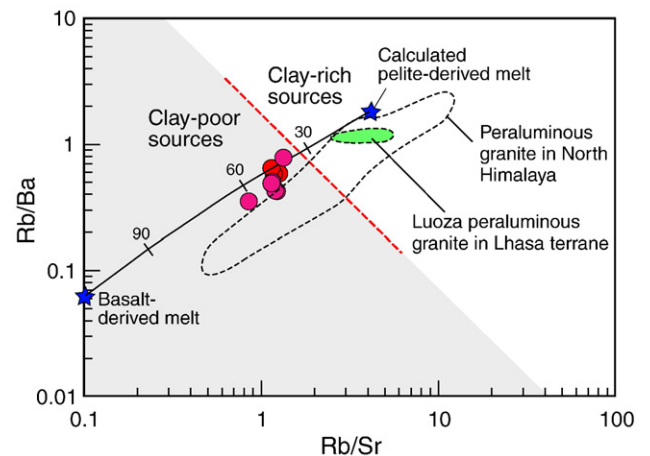


Fig. 6. Rb/Ba vs. Rb/Sr plot of Sylvester (1998) for the Pikang granites in the Lhasa terrane. Other data are the same in Fig. 4.

- (1) Major and trace element data for the Pikang granites are more consistent with a hybrid origin. The high CaO/Na₂O (>0.3), low Rb/Sr and Rb/Ba ratios of the Pikang granites indicate an origin of melts derived from plagioclase-rich and clay-poor sources (Fig. 6), which can be interpreted compositionally as resulting from pelite-derived melts that have mixed with mafic magmas (Sylvester, 1998).
- (2) Sr and Nd isotopic ratios of the Pikang granites (Fig. 5) preclude them from being simple melts of typical crustal materials. The Pikang granites have lower initial ⁸⁷Sr/⁸⁶Sr ratios and higher ε_{Nd(t)} values than the middle-upper crustal materials in the Lhasa terrane represented by the Amdo orthogneiss (⁸⁷Sr/⁸⁶Sr_(263 Ma) = 0.7237 to 0.7349; ε_{Nd(263 Ma)} = -6.6 to -8.8; Xu et al., 1985), Late Paleozoic siltstone (ε_{Nd(263 Ma)} = -17.0 to -13.0, Harris et al., 1988), and Early Jurassic strongly peraluminous granites in Ningzhong area (ε_{Nd(190 Ma)} = -14.1 to -11.6, Liu et al., 2006a). These observations suggest the involvement of a mantle component in the petrogenesis of the Pikang granites. As illustrated in Fig. 5, by assuming (i) the Early Jurassic peraluminous granites in Ningzhong area represent isotopically the composition of Lhasa terrane crustal melts (see Liu et al., 2006a) and (ii) the depleted component is represented by the Middle Permian Leiqingla high-alumina basalts in the same belt (Fig. 1b; Zhu et al., submitted for publication-b), it is suggested that melting of the crustal materials alone cannot explain the isotopic composition of the Pikang granites, but require ~30% contributions of basaltic melt (Fig. 5).
- (3) Zircon Hf isotopic compositions also support a hybrid origin for the Pikang granites. The ε_{Hf(t)} values (-4.5 to +1.9, Table 3) of ~263 Ma zircons from sample PK01-1 are close to those of chondritic uniform reservoir (CHUR) and near the upper limit of crust-derived melts (Fig. 3a) represented by the Late Triassic peraluminous granites in Luoza area of the central Lhasa terrane (-16.8 to -3.3; Zhu et al., submitted for publication-a). On the other hand, the Hf isotope crustal model ages of ~263 Ma zircons (T_{DM} = 1.2–1.6 Ga) are younger than those of the majority of inherited zircons in the same sample and older than those of the Early Jurassic Wuyu granitoids that were interpreted to be derived from a juvenile mantle source region (Chu et al., 2006) (Fig. 3b). These observations and inference also require the involvement of a mantle component (i.e., basalts) in the petrogenesis of the Pikang granites.

We found mixing of ~30% of mantle-derived melt and ~70% upper crustal-derived melt is needed to explain the isotopic compositions of the Pikang granites (Fig. 5). Petrological, geochemical and experimental studies for strongly peraluminous granites have shown that the heat for crustal melting is primarily provided by mantle-derived magmas that are then mixed with induced crustal melts (e.g., Patino Douce, 1995; Muir et al., 1996; Keay et al., 1997; Healy et al., 2004). Recent studies have suggested that the Early to Middle Permian high-alumina basalts in the central Lhasa terrane (e.g., Leiqingla basalt) were generated by partial melting of metasomatized peridotitic mantle wedge in an island-arc setting (Zhu et al., submitted for publication-b). In such a tectonic setting, mantle-derived magmas will remain in the crust (Bergantz, 1989) and will provide heat for crustal melting to produce granitoid magmas. Such a process appears to be the probable mechanism for the generation of the Pikang granites, which were emplaced soon after the Middle Permian Leiqingla arc volcanism as indicated by the SHRIMP zircon U–Pb age data (Zhu et al., submitted for publication-b; this study).

5.2. Permian collisional orogeny in the Lhasa terrane

Geochemical data suggest that the Pikang granites are strongly peraluminous S-type granite, reflecting both source material control

and controls of tectonic settings (e.g., syn- vs. post-collisional) in which the magmas form (e.g., Pearce et al., 1984; Liegeois et al., 1998; Sylvester, 1998; Barbarin, 1999; Patino Douce, 1999). Our calculation (see Fig. 5) suggests that isotopically the Pikang granites require ~30% mantle derived material (e.g., basaltic melt) and ~70% upper continental crustal material. The latter can either be terrigenous sediments (i.e., the mature upper continental crustal materials) or mature upper crust itself. The “coexistence” of mature continental crust and mantle derived melt (e.g., Leiqingla basaltic melt) in space and time requires a tectonic setting that resembles active continental margins. That is, subduction of oceanic lithosphere beneath mature continental lithosphere leads to mantle wedge melting that produces basaltic melt. This mantle melt will underplate or intrude the overlying mature continental crust, causing crustal melting and forming hybrid melts parental to granitoids like the highly evolved Pikang granites. This recorded (mantle and crustal) magmatism may have taken place at the stage towards an ocean closing and terrane collision. These interpretations are consistent with observations (see Fig. 5) as elaborated below.

The paleontologically age-constrained Early Permian high-alumina basalts in Jiangrang, Nixiong areas and andesites in Ranwu area, along with the Middle Permian volcanic rocks in Leiqingla area along the southern margin of the central Lhasa terrane (Fig. 1a and b), which are most consistent with being genetically associated with a continental arc setting (Pan et al., 2006; Zhu et al., submitted for publication-b), precede the emplacement of the Pikang granites. Recent studies have also shown that the Middle Permian limestones were overlain by the Upper Permian clastic rocks with angular unconformity (Fig. 7) observed in western Jiangrang (Zhou et al., 2002), Nixiong (Xie et al., 2003), central Liwo (Lu et al., 2002; Wang et al., 2004) and Leiqingla (Wu et al., 2003) of the central Lhasa terrane (Fig. 1b). The timing of the tectonic event recorded by the regional angular unconformity is effectively synchronous with the emplacement of the Pikang granites and the very high-pressure metamorphism (occurred at ~262 Ma) revealed by the Songdo eclogite (Fig. 1b) interpreted as remnant of Paleo-Tethyan oceanic lithosphere (Yang et al., 2009). Note that the eclogite that can be exhumed to the surface approximates the last bit of subducting/subducted oceanic lithosphere before collision and exhumation. Hence, the metamorphic age of the eclogite represents onset of the collision. All these data and reasoning together with the sedimentary and tectonic record point to an orogenic event extending

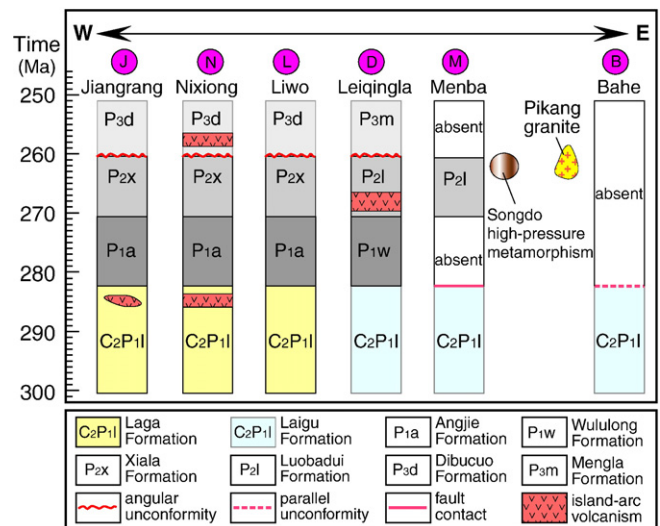


Fig. 7. Space–time diagram showing the Upper Carboniferous–Upper Permian sedimentary, tectonic, metamorphic and magmatic history of the central Lhasa terrane (Lu et al., 2002; Xie et al., 2003; Jiang et al., 2003; Wu et al., 2003; Yin et al., 2003; Wang et al., 2004; Yang et al., 2005; Yang et al., 2009; this study). Pink circles with letter denote section localities shown in Fig. 1b.

E–W for ~1000 km from western Coqen to eastern Gongbo Gyamda (Fig. 7) in the central Lhasa terrane. We thus propose that the Pikang peraluminous granite magmatism, the regional angular unconformity between the Middle and the Upper Permian, and the Songdo eclogite of the same metamorphic age (~262 Ma) to represent different products of a common event in time and space soon after the eruption of the Middle Permian Leiqingla arc lavas. We refer this newly recognized event as “the Permian Gangdese Orogeny” (vs. Late Triassic, Early Jurassic and Cretaceous orogenic events already recognized in the Lhasa terrane).

5.3. Implications

The Lhasa terrane has long been considered as part of Gondwana and traditionally placed adjacent to Greater India in popular Paleozoic reconstructions, depicting a vast shallow marine sea from Qiangtang terrane via Lhasa terrane to the Greater India and Himalaya (Dewey et al., 1988; Leeder et al., 1988; Golonka and Ford, 2000; Metcalfe, 2002). The Pikang granite of ~263 Ma identified in this study, the regional angular unconformity recently recognized between the Middle Permian and the Upper Permian (Fig. 7), and the contemporaneous high-pressure metamorphism (Yang et al., 2009), provide strong evidence for the event of the Permian Gangdese Orogeny in the Lhasa terrane (Fig. 1b). These observations combined with the Early to Middle Permian arc-type magmatism (Zhu et al., submitted for publication-b) suggest a compressional regime from subduction to syn-collision in the Lhasa terrane rather than an extensional tectonic regime related to the separation of the Qiangtang terrane from Gondwana during the Permian as previously thought (Dewey et al., 1988; Leeder et al., 1988; Yin and Harrison, 2000; Booth et al., 2004; Kapp et al., 2005; Leier et al., 2007). The compressional tectonic regime in the Lhasa terrane differs distinctly from the Tethyan Himalaya to the

south and the Qiangtang terrane to the north in having extensional tectonic regime during the Permian (Deng et al., 1996; Garzanti et al., 1999; Yin and Harrison, 2000; Zhu et al., submitted for publication-b). Such a difference results in two new hypotheses regarding tectonic reconstructions of the Lhasa terrane during the Permian.

Some authors proposed that the Lhasa terrane should be taken out from the continuous Paleozoic Qiangtang–Lhasa–Himalaya reconstructions (Golonka and Ford, 2000; Metcalfe, 2002), and be placed adjacent to the northern margin of Australia (Ferrari et al., 2008). Argument for this model is based on the presence of late Carboniferous/early Permian Dagze arc magmatism re-interpreted from the documentation by Pearce and Mei (1988) in the Lhasa terrane. The arc magmatism was attributed to southward subduction of the Paleo-Tethyan oceanic lithosphere with the consequent back-arc opening of the Eastern Neo-Tethys (Ferrari et al., 2008). Such a geodynamic regime, however, does not account for the Songdo eclogite that is exposed in the southern margin of the central Lhasa terrane (Fig. 1b). An alternative model for the Lhasa terrane was recently proposed by Zhu et al. (submitted for publication-b), who suggested that the Lhasa terrane could be considered as a separate intra-oceanic tectonic block (or a micro-continent) in the Paleo-Tethyan Ocean during Carboniferous–Permian times, and was subjected to the northward subduction of the Paleo-Tethyan oceanic lithosphere along its southern margin during the Early to Middle Permian (Fig. 8a and b). This suggestion is inferred from the coexistence of the Early to Middle Permian arc-type magmatism in the Lhasa terrane and the extension-type magmatism in the Tethyan Himalaya. Likewise, such an alternative model can now be updated to account for the Permian Pikang peraluminous granite.

The Pikang granite magmatism is interpreted to record a syn-collisional orogenic event in the Lhasa terrane at ~263 Ma. Indeed, the Songdo eclogite may record the subduction and closing of the Carboniferous–Permian Paleo-Tethyan Ocean south of the Lhasa

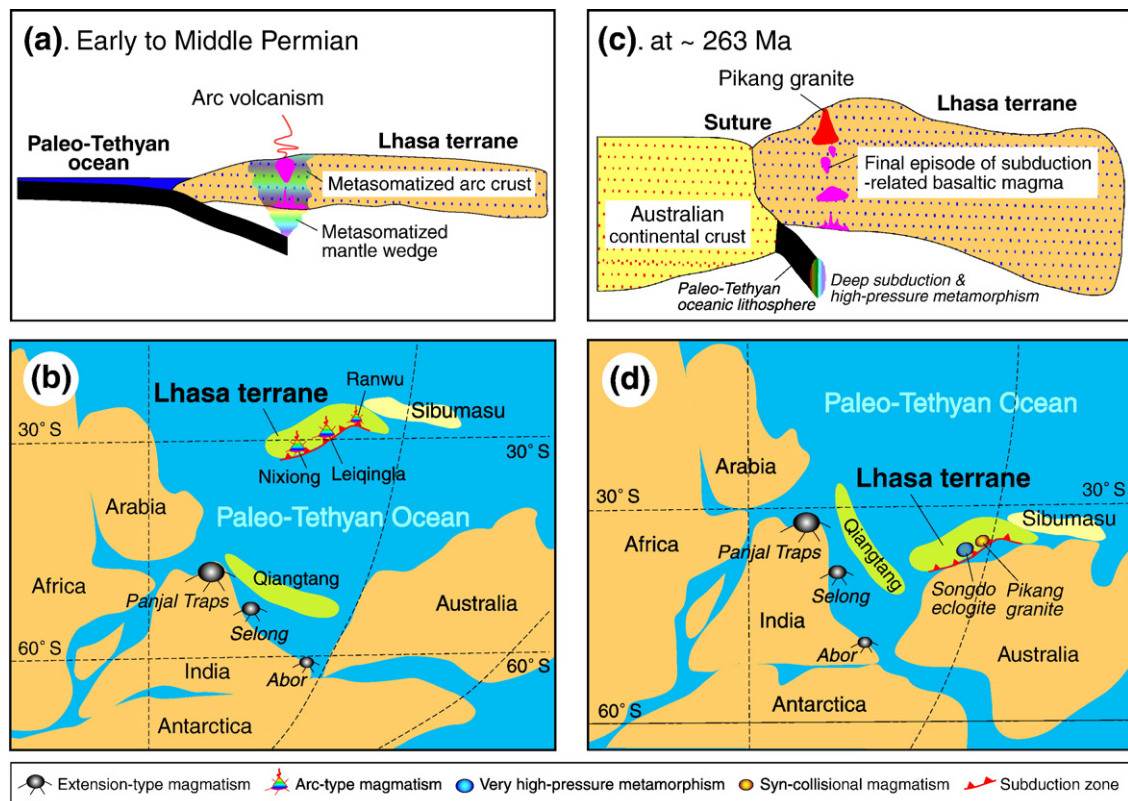


Fig. 8. (a) Schematic section for the generation of Early to Middle Permian volcanic rocks in the Lhasa terrane. (b) Tectonic reconstruction illustrating the Lhasa terrane located within the Paleo-Tethyan Ocean as a micro-continent during the Early to Middle Permian (Zhu et al., submitted for publication-b). (c) Schematic representation for the generation of the Pikang granites in a thickened crust of the Lhasa terrane at ~263 Ma. Not drawn to scale. (d) An integrated reconstruction model for the Lhasa terrane at ~263 Ma that accounts for all published data and observations (Zhu et al., submitted for publication-b; Yang et al., 2009; this study).

terrane (Yang et al., 2007, 2009). An important issue for the Permian collision event is with which continental block the Lhasa terrane may have collided with at this time. Although shortening structures potentially related to the Permian Gangdese Orogeny in the Lhasa terrane requires further investigations, collision-induced crustal thickening would be expected (Sylvester, 1998). This requires that the unknown continental block should have ancient lithospheric root to support its overlying crust (e.g., Jordan, 1988; Niu et al., 2003) when collided with the Lhasa terrane. Furthermore, the unknown block should have been located to the south of the Lhasa terrane, because the Pikang granites are exposed in the southern margin of the terrane. According to palinspastic reconstruction for the northern margin of eastern Gondwana (Enkin et al., 1992; Ziegler et al., 1997; Scotese et al., 1999; Ferrari et al., 2008; Zhu et al., submitted for publication-b), the likely candidate block is the Australian continent, rather than the Tethyan Himalaya that was under extension at the time of Permian Lhasa terrane collision (Garzanti et al., 1999; Zhu et al., submitted for publication-b).

On the basis of the latest data on the magmatic history (including data reported here), the regional angular unconformity (Fig. 7), and the subduction-zone metamorphism (Yang et al., 2009), we tentatively propose an updated reconstruction model for the Lhasa terrane during the Permian (Fig. 8): (1) The Lhasa terrane may represent a micro-continent situated within the Paleo-Tethyan Ocean during the Carboniferous–Middle Permian time. The Paleo-Tethyan Oceanic lithosphere was subducted northward beneath the Lhasa terrane during the Early to Middle Permian and led to the production of the arc-like volcanic rocks recorded in Jiangrang, Nixiong, Leiqingla, and Ranwu areas along the southern margin of the central Lhasa terrane (Zhu et al., submitted for publication-b) (Fig. 8a and b). (2) The Lhasa terrane with arc affinity probably collided with the northern margin of Australia at ~263 Ma and led to the closure of the Paleo-Tethyan Ocean as also recorded by the Songdo eclogite (Yang et al., 2009). During the collision, the final episode of subduction-related basaltic magmatism provided heat for thickened upper crustal melting and mixed with crust-derived melts to form hybrid melts parental to the evolved Pikang peraluminous granites (Fig. 8c and d). Our model suggests that the Lhasa terrane moved significantly southward from the Early to the latest Middle Permian, which is supported by recent paleomagnetic data for the sedimentary sequences of the Lower Permian Angjie and Middle Permian Xiala Formations in the Lhasa terrane (Wang and Ran, personal communication, 2008).

6. Conclusions

- (1) Zircon U–Pb isotopic data reveal that the Pikang granite in the Lhasa terrane was emplaced at about 263 Ma, coeval with the eclogite metamorphism and regional angular unconformity recently identified in the terrane.
- (2) Zircons from the Pikang granites show narrow variation in Hf isotopic compositions ($\varepsilon_{\text{Hf}(t)} = -4.5$ to $+1.9$), significantly higher than melts derived from mature continental crustal materials, suggesting mantle input to the granitoid magmatism.
- (3) The Pikang granites are strongly peraluminous (i.e., typical S-type granites) characterized by high A/CNK values (≥ 1.08), high normative corundum (1.3–2.0%), moderately negative Eu anomalies ($\text{Eu}/\text{Eu}^* = 0.48\text{--}0.61$), and strongly negative Ba, Nb, Sr, P and Ti anomalies. They have high $\varepsilon_{\text{Nd}(t)}$ values (-6.4 to -6.0) and low initial $^{87}\text{Sr}/^{86}\text{Sr}$ ratios (0.7082–0.7096) relative to melts derived from mature continental crust materials.
- (4) Hf isotopic and trace element data of zircons coupled with whole-rock geochemical data indicate that melts parental to the Pikang granites can be generated by mixing between predominantly Al_2O_3 -rich lithologies (e.g., terrigenous sediments or *in situ* upper crustal materials) and minor mantle-derived basaltic melts.

- (5) The Pikang granite magmatism and regional angular unconformity between the Middle Permian and the Upper Permian are consistent with a synclinal orogeny that is referred to here as “the Permian Gangdese Orogeny” in the Lhasa terrane at ~263 Ma.
- (6) The Permian Gangdese Orogeny is interpreted as resulting from the collision between the Lhasa terrane and the northern margin of Australia in response to the closure of Paleo-Tethyan Ocean south of the Lhasa terrane.

Acknowledgements

The research was supported by the Excellent Young Scientists Programme of the Ministry of Land and Resources (to Di-Cheng), Chinese NSF (40572051, and 40503005), the Chinese 111 Project (No. B0701), and the programme of the Integrated Study of Basic Geology of Qinghai–Tibetan Plateau of the China Geological Survey. Y. N. thanks a Leverhulme Trust for a Research Fellowship. We thank Meng-Ning Dai and Chun-Lei Ning for helping with XRF, ICP-MS and Sr–Nd isotopic analyses of samples; Cheng-Shan Wang, Bo Ran, Ben-Pei Liu, and Xiang Zhou for the useful discussions about paleogeography; two anonymous reviewers for the constructive comments that greatly improved the quality of this manuscript; and Editor Mian Liu for editorial handling.

References

- Andersen, T., 2002. Correction of common lead in U–Pb analyses that do not report ^{204}Pb . *Chemical Geology* 192, 59–79.
- Barbarin, B., 1999. A review of the relationships between granitoid types, their origins and their geodynamic environments. *Lithos* 46, 605–626.
- Bergantz, G.W., 1989. Underplating and partial melting: implications for melt generation and extraction. *Science* 245, 1093–1095.
- Blichert-Toft, J., Albarède, F., 1997. The Lu–Hf geochemistry of chondrites and the evolution of the mantle–crust system. *Earth and Planetary Science Letters* 148, 243–258.
- Bonin, B., 1998. Alkaline rocks and geodynamics. *Turkish Journal of Earth Sciences* 7, 105–118.
- Booth, A.L., Zeitler, P.K., Kidd, W.S.F., Wooden, J., Liu, Y.P., Idleman, B., Hren, M., Chamberlain, C.P., 2004. U–Pb zircon constraints on the tectonic evolution of Southeastern Tibet, Namche Barwa area. *American Journal of Science* 304, 889–929.
- Chu, M.F., Chung, S.L., Song, B., Liu, D.Y., O'Reilly, S.Y., Pearson, N.J., Ji, J.Q., Wen, D.J., 2006. Zircon U–Pb and Hf isotope constraints on the Mesozoic tectonics and crustal evolution of southern Tibet. *Geology* 34, 745–748.
- Chung, S.L., Chu, M.F., Zhang, Y.Q., Xie, Y.W., Lo, C.H., Lee, T.Y., Lan, C.Y., Li, X.H., Zhang, Q., Wang, Y.Z., 2005. Tibetan tectonic evolution inferred from spatial and temporal variations in post-collisional magmatism. *Earth-Science Reviews* 68, 173–196.
- Copeland, P., Harrison, T.M., Pan, Y., Kidd, W.S.F., Roden, M., Zhang, Y.Q., 1995. Thermal evolution of the Gangdese batholith, southern Tibet: a history of episodic unroofing. *Tectonics* 14, 223–236.
- Coulon, C., Maluski, H., Bollinger, C., Wang, S., 1986. Mesozoic and Cenozoic volcanic rocks from central and southern Tibet: $^{39}\text{Ar}/^{40}\text{Ar}$ dating, petrological characteristics and geodynamical significance. *Earth and Planetary Science Letters* 79, 281–302.
- Deng, W.M., Yin, J.X., Guo, Z.P., 1996. Basic-ultramafic and volcanic rocks in Chagbu-Shuanghu area of northern Xizang (Tibet), China. *Science in China (series D)* 39, 359–368.
- Dewey, J.F., Shackleton, R.M., Chang, C.F., Sun, Y.Y., 1988. The tectonic evolution of the Tibetan plateau. *Philosophical Transactions of the Royal Society of London, Series A: Mathematical and Physical Sciences* 327, 379–413.
- England, P., Searle, M., 1986. The Cretaceous–Tertiary deformation of the Lhasa block and its implications for crustal thickening in Tibet. *Tectonics* 5, 1–14.
- Enkin, R.J., Yang, Z.Y., Chen, Y., Courtillot, V., 1992. Paleomagnetic constraints on the geodynamic history of the major blocks of China from the Permian to the present. *Journal of Geophysical Research* 97 (B10), 13953–13989.
- Eyal, M., Litvinovsky, B.A., Katzir, Y., Zanzivilevich, A.N., 2004. The Pan-African high-K calc-alkaline peraluminous Elat granite from southern Israel: geology, geochemistry and petrogenesis. *Journal of African Earth Sciences* 40, 115–136.
- Ferrari, O.M., Hochard, C., Stampfli, G.M., 2008. An alternative plate tectonic model for the Palaeozoic–Early Mesozoic Palaeotethyan evolution of Southeast Asia (Northern Thailand–Burma). *Tectonophysics* 451, 346–365.
- Gao, S., Liu, X.M., Yuan, H.L., Hattendorf, B., Gunther, D., Chen, L., Hu, S.H., 2002. Determination of forty-two major and trace elements in USGS and NIST SRM glasses by laser ablation-inductively coupled plasma-mass spectrometry. *Geostandards Newsletter – Journal of Geostandards and Geoanalysis* 26, 191–196.
- Garzanti, E., Le Fort, P., Sciunnach, D., 1999. First report of Lower Permian basalts in South Tibet: tholeiitic magmatism during break-up and incipient opening of Neotethys. *Journal of Asian Earth Sciences* 17, 533–546.

- Golonka, J., 2007. Late Triassic and Early Jurassic palaeogeography of the world. *Palaeogeography, Palaeoclimatology, Palaeoecology* 244, 297–307.
- Golonka, J., Ford, D., 2000. Pangean (Late Carboniferous–Middle Jurassic) paleoenvironment and lithofacies. *Palaeogeography, Palaeoclimatology, Palaeoecology* 161, 1–34.
- Griffin, W.L., Pearson, N.J., Belousova, E., Jackson, S.E., van Acherbergh, E., O'Reilly, S.Y., Shee, S.R., 2000. The Hf isotope composition of cratonic mantle: LAM-MC-ICPMS analysis of zircon megacrysts in kimberlites. *Geochimica et Cosmochimica Acta* 64, 133–147.
- Griffin, W.L., Wang, X., Jackson, S.E., Pearson, N.J., O'Reilly, S.Y., Xu, X., Zhou, X., 2002. Zircon chemistry and magma mixing, SE China: in-situ analysis of Hf isotopes, Tonglu and Pingtan igneous complexes. *Lithos* 61, 237–269.
- Guynn, J.H., Kapp, P., Pullen, A., Gehrels, G., Heizler, M., Ding, L., 2006. Tibetan basement rocks near Amdo reveal “missing” Mesozoic tectonism along the Bangong suture, central Tibet. *Geology* 34, 505–508.
- Harris, N.B.W., Xu, R.H., Lewis, C.L., Hawkesworth, C.J., Zhang, Y.Q., 1988. Isotope geochemistry of the 1985 Tibet Geotraverse: Lhasa to Golmud. *Philosophical Transactions of the Royal Society of London, Series A: Mathematical and Physical Sciences* 327, 263–285.
- He, S.D., Kapp, P., DeCelles, P.G., Gehrels, G.E., Heizler, M., 2007. Cretaceous–Tertiary geology of the Gangdese Arc in the Linzhou area, southern Tibet. *Tectonophysics* 433, 15–37.
- Healy, B., Collins, W.J., Richards, S.W., 2004. A hybrid origin for Lachlan S-type granites: the Murrumbidgee Batholith example. *Lithos* 78, 197–216.
- Hu, D.G., Wu, Z.H., Jiang, W., Shi, Y.R., Ye, P.S., Liu, Q.S., 2005. SHRIMP zircon U–Pb age and Nd isotopic study on the Nyainqentanglha Group in Tibet. *Science in China (Series D-Earth Sciences)* 48, 1377–1386.
- Ji, Z.S., Yao, J.X., Wu, G.C., 2007. Stratigraphic division of the marine Triassic in the Coqen area, western Gangdese, Tibet, China. *Geological Bulletin of China* 26, 947–952 (in Chinese with English abstract).
- Jiang, Y.S., Zhou, Y.Y., Li, J.B., Xie, Y.X., Gou, Y.D., Peng, B., Wang, M.G., Zhu, S.H., 2003. 1: 250, 000 geological report of Coqen District with geological map. Institute of Sichuan Geological Survey Chengdu, unpublished (in Chinese).
- Jordan, T.H., 1988. Structure and formation of the continental lithosphere. *Journal of Petrology* 11–37 (Special Lithosphere Issue).
- Kapp, P., Yin, A., Harrison, T.M., Ding, L., 2005. Cretaceous–Tertiary shortening, basin development, and volcanism in central Tibet. *Geological Society of America Bulletin* 117, 865–878. doi:10.1130/B25595.1.
- Kapp, P., DeCelles, P.G., Leier, A.L., Fabijanic, J.M., He, S., Pullen, A., Gehrels, G.E., 2007. The Gangdese retro-arc thrust belt revealed. *GSA Today* 17, 4–9.
- Keay, S., Collins, W.J., McCulloch, M.T., 1997. A three-component Sr–Nd isotopic mixing model for granitoid genesis, Lachlan Fold Belt, eastern Australia. *Geology* 25, 307–310.
- Keto, L.S., Jacobsen, S.B., 1987. Nd and Sr isotopic variations of Early Paleozoic oceans. *Earth and Planetary Science Letters* 84, 27–41.
- Leeder, M.R., Smith, A.B., Yin, J.X., 1988. Sedimentology, palaeoecology and palaeoenvironmental evolution of the 1985 Lhasa to Golmud Geotraverse. *Royal Society of London Philosophical Transactions, Series A* 327, 107–143.
- Leier, A.L., Kapp, P., Gehrels, G.E., DeCelles, P.G., 2007. Detrital zircon geochronology of Carboniferous–Cretaceous strata in the Lhasa terrane, Southern Tibet. *Basin Research* 19, 361–378.
- Li, Z.L., Yang, J.S., Luo, L.Q., Li, T.F., Xu, X.Z., Ren, Y.F., 2008. Geochemical characteristics, Sm–Nd and Rb–Sr isotopic compositions of newly-discovered eclogite in the Lhasa terrane, Tibet and their geological significance. *Acta Geologica Sinica* 82, 941–948 (in Chinese with English abstract).
- Liegeois, J.P., Navez, J., Hertogen, J., Black, R., 1998. Contrasting origin of post-collisional high-K calc-alkaline and shoshonitic versus alkaline and peralkaline granitoids: the use of sliding normalization. *Lithos* 46, 1–28.
- Liu, Q.S., Jiang, W., Jian, P., Ye, P.S., Wu, Z.H., Hu, D.G., 2006a. The zircon SHRIMP U–Pb age and petrochemical and geochemical features of Mesozoic muscovite monzogranite at Ningzhong, Tibet. *Acta Petrologica Sinica* 22, 643–652 (in Chinese with English abstract).
- Liu, D.Y., Jian, P., Kröner, A., Xu, S.T., 2006b. Dating of prograde metamorphic events deciphered from episodic zircon growth in rocks of the Dabie–Sulu UHP complex, China. *Earth and Planetary Science Letters* 250, 650–666.
- Lu, S.W., Du, F.J., Ren, J.D., Zhang, Y.Q., Liu, P.D., Pei, Z.C., Jia, G.X., Xie, C.Y., Li, X.Z., 2002. 1: 250, 000 geological report of Rebuka region with geological map. Institute of Henan Geological Survey, Zhengzhou, unpublished (in Chinese).
- Maluski, H., Proust, F., Xiao, X.C., 1982. ³⁹Ar/⁴⁰Ar dating of the trans-Himalayan calc-alkaline magmatism of southern Tibet. *Nature* 298, 152–154.
- Metcalfe, I., 2002. Permian tectonic framework and palaeogeography of SE Asia. *Journal of Asian Earth Sciences* 20, 551–566.
- Mo, X.X., Hou, Z.Q., Niu, Y.L., Dong, G.C., Qu, X.M., Zhao, Z.D., Yang, Z.M., 2007. Mantle contributions to crustal thickening during continental collision: evidence from Cenozoic igneous rocks in southern Tibet. *Lithos* 96, 225–242.
- Muir, R.J., Weaver, S.D., Bradshaw, J.D., Eby, G.N., Evans, J.A., 1996. Geochemistry of the Karamea Batholith, New Zealand and comparisons with the Lachlan Fold Belt granites of SE Australia. *Lithos* 39, 1–20.
- Murphy, M.A., Yin, A., Harrison, T.M., Dürr, S.B., Chen, Z., Ryerson, F.J., Kidd, W.S.F., Wang, X., Zhou, X., 1997. Did the Indo-Asian collision alone create the Tibetan plateau? *Geology* 25, 719–722.
- Niu, Y., O'Hara, M.J., Pearce, J.A., 2003. Initiation of subduction zones as a consequence of lateral compositional buoyancy contrast within the lithosphere: a petrological perspective. *Journal of Petrology* 44, 851–866.
- Pan, G.T., Ding, J., 2004. Geological map (1:1500000) of Qinghai–Xizang (Tibetan) Plateau and adjacent areas. Chengdu Cartographic Publishing House, Chengdu, pp. 1–133.
- Pan, G.T., Mo, X.X., Hou, Z.Q., Zhu, D.C., Wang, L.Q., Li, G.M., Zhao, Z.D., Geng, Q.R., Liao, Z.L., 2006. Spatial–temporal framework of the Gangdese Orogenic Belt and its evolution. *Acta Petrologica Sinica* 22, 521–533 (in Chinese with English abstract).
- Patino Douce, A.E., 1995. Experimental generation of hybrid silicic melts by reaction of high Al basalt with metamorphic rocks. *Journal of Geophysical Research* 100, 623–639.
- Patino Douce, A.E., 1997. Generation of peraluminous A-type granites by low-pressure melting of calc-alkaline granitoids. *Geology* 25, 743–766.
- Patino Douce, A.E., 1999. What do experiments tell us about the relative contributions of crust and mantle to the origin of granitic magmas? In: Castro, A., Fernandez, C., Vigneresse, J.L. (Eds.), *Understanding Granites: Integrating New and Classical Techniques*. Geological Society Special Publications, vol. 168, pp. 55–75.
- Pearce, J.A., Mei, H.J., 1988. Volcanic rocks of the 1985 Tibet Geotraverse: Lhasa to Golmud. *Philosophical Transactions of the Royal Society of London, Series A: Mathematical and Physical Sciences* 327, 169–201.
- Pearce, J.A., Harris, N.B., Tindle, A.G., 1984. Trace element discrimination diagrams for the tectonic interpretation of granitic rocks. *Journal of Petrology* 25, 956–983.
- Scotese, C.R., 2004. A continental drift flipbook. *Journal of Geology* 112, 729–741.
- Scotese, C.R., Boucot, A.J., McKerrow, W.S., 1999. Gondwanan palaeogeography and palaeoclimatology. *Journal of African Earth Sciences* 28, 99–114.
- Soderlund, U., Patchett, P.J., Vervoort, J.D., Isachsen, C.E., 2004. The ¹⁷⁶Lu decay constant determined by Lu–Hf and U–Pb isotope systematics of Precambrian mafic intrusions. *Earth and Planetary Science Letters* 219, 311–324.
- Stampfli, G.M., Borel, G.D., 2002. A plate tectonic model for the Paleozoic and Mesozoic constrained by dynamic plate boundaries and restored synthetic oceanic isochrons. *Earth and Planetary Science Letters* 196, 17–33.
- Sun, S.S., McDonough, W.F., 1989. Chemical and isotope systematics of oceanic basalts: implications for mantle composition and processes. In: Saunders, A.D. (Ed.), *Magmatism in ocean Basins*. Geological Society Publication, vol. 42, pp. 313–345.
- Sylvester, P.J., 1998. Postcollisional strongly peraluminous granites. *Lithos* 45, 29–44.
- Wang, L.Q., Zhu, D.C., Pan, G.T., 2004. Primary results and progress of regional geological survey (1: 250,000): the south of Qinghai–Tibet Plateau. *Geological Bulletin of China* 23, 413–420 (in Chinese with English abstract).
- Wang, C.S., Zhao, X.X., Liu, Z.F., Lippert, P.C., Graham, S.A., Coe, R.S., Yi, H.S., Zhu, L.D., Liu, S., Li, Y.L., 2008. Constraints on the early uplift history of the Tibetan Plateau. *PNAS* 105, 4987–4992.
- Wen, D.R., Liu, D.Y., Chung, S.L., Chu, M.F., Ji, J.Q., Zhang, Q., Song, B., Lee, T.Y., Yeh, M.W., Lo, C.H., 2008a. Zircon SHRIMP U–Pb ages of the Gangdese Batholith and implications for Neotethyan subduction in southern Tibet. *Chemical Geology* 252, 191–201.
- Wen, D.R., Chung, S.L., Song, B., Iizuka, Y., Yang, H.J., Ji, J.Q., Liu, D.Y., Gallet, S., 2008b. Late Cretaceous Gangdese intrusions of adakitic geochemical characteristics, SE Tibet: Petrogenesis and tectonic implications. *Lithos* 105, 1–11.
- White, A.J.R., Chappell, B.W., 1988. Some supracrustal S-type granites of the Lachlan Fold Belt. *Transactions of the Royal Society of Edinburgh: Earth Sciences* 79, 169–181.
- Wu, F.Y., Yang, Y.H., Xie, L.W., Yang, J.H., Xu, P., 2006. Hf isotopic compositions of the standard zircons and baddeleyites used in U–Pb geochronology. *Chemical Geology* 234, 105–126.
- Wu, Z.H., Meng, X.G., Hu, D.G., Jiang, W., Ye, P.S., Zhu, D.G., Liu, Q.S., Yang, X.D., Zhao, Z.G., Wu, Z.H., Zhao, X.T., Wang, J.P., Feng, X.Y., Ji, Z.S., 2003. 1: 250, 000 geological report of Dangxiang region with geological map. Institute of Geomechanics, Chinese Academy of Geological Sciences Beijing, unpublished (in Chinese).
- XBGMR (Xizang Bureau of Geology and Mineral Resources), 1991. *The Regional Geology of Xikazi and Yadong (Geology Part) Scale 1: 200000*. Geological Publishing House, Beijing, pp. 22–148 (in Chinese).
- Xie, L.W., Zhang, Y.B., Zhang, H.H., Sun, J.F., Wu, F.Y., 2008. In situ simultaneous determination of trace elements, U–Pb and Lu–Hf isotopes in zircon and baddeleyite. *Chinese Science Bulletin* 53, 1565–1573.
- Xie, G.G., Zhou, A.J., Yuan, J.Y., Liao, S.P., Li, X.Y., Tang, F.L., Xu, Z.F., Chen, Z.H., Luo, X.C., Xu, Y.B., Xiao, Y.B., Cao, S.H., Huang, C.G., 2003. 1: 250, 000 geological report of Comai region with geological map. Institute of Jiangxi Geological Survey, Nanchang, unpublished (in Chinese).
- Xu, R.H., Schärer, U., Allègre, C.J., 1985. Magmatism and metamorphism in the Lhasa block (Tibet): a geochronological study. *Journal of Geology* 93, 41–57.
- Yang, J.S., Xu, Z.Q., Li, Z.L., Li, H.Q., Li, T.F., Ren, Y.F., Xu, X.Z., Chen, S.Y., 2007. Oceanic subduction-type eclogite in the Lhasa block, Tibet, China: remains of the Paleotethys ocean basin? *Geological Bulletin of China* 26, 1277–1287 (in Chinese with English abstract).
- Yang, J.S., Xu, Z.Q., Li, Z.L., Xu, X.Z., Li, T.F., Ren, Y.F., Li, H.Q., Chen, S.Y., Robinson, P.T., 2009. Discovery of an eclogite belt in the Lhasa block, Tibet: A new border for Paleotethys? *Journal of Asian Earth Sciences* 34, 76–89.
- Yang, D.M., He, Z.H., Wang, T.W., Wu, S.Z., Deng, J.X., Dong, Q.S., Huang, Y.C., Zheng, C.Q., Zhao, L., Dai, L.N., Wang, J., 2005. 1: 250, 000 geological report of Menba District with geological map. Institute of Jilin University Geological Survey, Changchun, unpublished (in Chinese).
- Yin, A., Harrison, T.M., 2000. Geologic evolution of the Himalayan–Tibetan orogen. *Annual Review of Earth and Planetary Sciences* 28, 211–280.
- Yin, J.X., Xu, J.T., Liu, C.J., Li, H., 1988. The Tibetan Plateau: regional stratigraphic context and previous work. *Philosophical Transactions of the Royal Society of London, Series A, Mathematical and Physical Sciences* 327, 5–52.
- Yin, A., Harrison, T.M., Ryerson, F.J., Chen, W.J., Kidd, W.S.F., Copeland, P., 1994. Tertiary structural evolution of the Gangdese thrust system, southeastern Tibet. *Journal of Geophysical Research* 99 (B9), 18175–18201.
- Yin, G.H., Chen, Y.M., Bao, J.Y., Hou, S.Y., Lu, Y., Duan, G.X., Zhang, J.Y., Liu, Z., Xiao, L., 2003. 1: 250, 000 geological report of Linzhi region with geological map. Institute of Yunnan Geological Survey, Kunming, unpublished (in Chinese).
- Zhang, H.F., Gao, S., Zhong, Z.Q., Zhang, B.R., Zhang, L., Hu, S.H., 2002. Geochemical and Sr–Nd–Pb isotopic compositions of Cretaceous granitoids: constraints on tectonic framework and crustal structure of the Dabieshan ultrahigh pressure metamorphic belt, China. *Chemical Geology* 186, 281–299.

- Zhang, H.F., Harris, N., Parrish, R., Kelley, S., Zhang, L., Rogers, N., Argles, T., King, J., 2004. Causes and consequences of protracted melting of the mid-crust exposed in the North Himalayan antiform. *Earth and Planetary Science Letters* 228, 195–212.
- Zhang, H.F., Xu, W.C., Guo, J.Q., Zong, K.Q., Cai, H.M., Yuan, H.L., 2007. Indosinian orogenesis of the Gangdese terrane: evidences from zircon U–Pb dating and petrogenesis of granitoids. *Earth Science – Journal of China University of Geoscience* 32, 155–166.
- Zhou, Y.Y., Jiang, Y.S., Wang, M.G., 2002. Permian Dibucuo Formation in the Coqen–Shenza stratigraphic area, Tibet. *Geological Bulletin of China* 21, 79–82 (in Chinese with English abstract).
- Zhu, D.C., Pan, G.T., Chun, S.L., Liao, Z.L., Wang, L.Q., Li, G.M., 2008a. SHRIMP zircon age and geochemical constraints on the origin of Early Jurassic volcanic rocks from the Yeba Formation, southern Gangdese in south Tibet. *International Geology Review* 50, 442–471.
- Zhu, D.C., Pan, G.T., Wang, L.Q., Mo, X.X., Zhao, Z.D., Zhou, C.Y., Liao, Z.L., Dong, G.C., Yuan, S.H., 2008b. Tempo-spatial variations of Mesozoic magmatic rocks in the Gangdese belt, Tibet, China, with a discussion of geodynamic setting-related issues. *Geological Bulletin of China* 27, 1535–1550 (in Chinese with English abstract).
- Zhu, D.C., Pan, G.T., Zhao, Z.D., Lee, H.Y., Kang, Z.Q., Liao, Z.L., Wang, L.Q., Li, G.M., Dong, G.C., Liu, B., 2009. Early Cretaceous subduction-related adakite-like rocks in the Gangdese, south Tibet: products of slab melting and subsequent melt-peridotite interaction? *Journal of Asian Earth Sciences* 34, 298–309.
- Zhu, D.C., Mo, X.X., Niu, Y.L., Zhao, Z.D., Chung, S.L., Wu, F.Y., Wang, L.Q., Hou, Z.Q., DePaolo, D.J., submitted for publication-a. The lithospheric architecture of the Lhasa Terrane: Revelation and geodynamic significance.
- Zhu, D.C., Mo, X.X., Zhao, Z.D., Niu, Y.L., Wang, L.Q., Chu, Q.H., Pan, G.T., Xu, J.F., Liu, Y., Zhou, C.Y., submitted for publication-b. Coexisting Permian extension- and arc-type magmatism in southern Tibet and paleogeographic implications. *Tectonics*.
- Ziegler, A.M., Hulver, M.L., Roeley, D.B., 1997. Permian world topography and climate. In: Martini, I.P. (Ed.), *Late glacial and postglacial environmental changes: quaternary, carboniferous-Permian and Proterozoic*. Oxford University Press, New York, pp. 111–146.